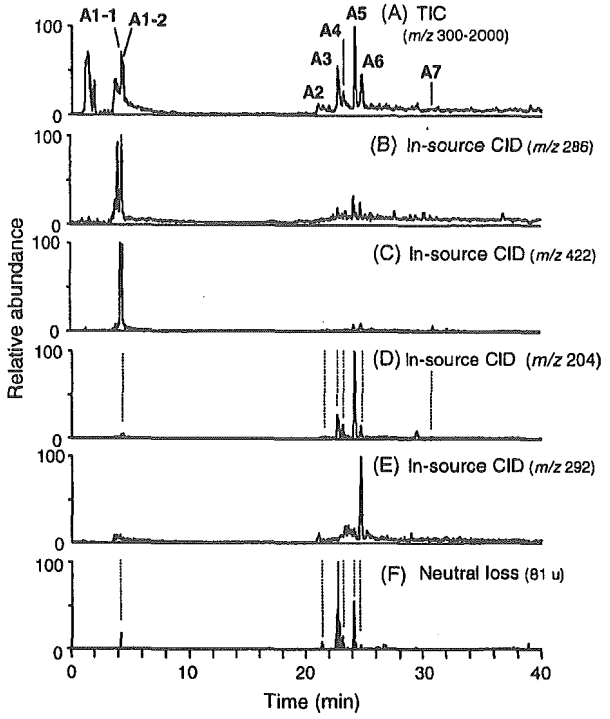

Fig. 6. Total ion chromatogram (TIC) of Asp-N digested protein at 20–25 kDa (*m/z* 300–2000) (A), mass chromatograms from TIC with in-source CID of *m/z* 286 (B), 422 (C), 204 (D), and 292 (E), and neutral loss chromatogram of 81 u by data-dependent CID-MS/MS (F).

ion spectra. Glycopeptides in peak T2 were characterized as Ala73-Lys78 glycosylated at Asn74 with *N*-glycans consisting of $dHex_{0-2}Hex_{3-6}HexNAc_{2-5}$. These *N*-glycans can be identified as high-mannose-type oligosaccharide (M5), and complex-type and hybrid-type oligosaccharides containing Fuc attached to inner trimannosyl core GlcNAc. Their structural assignments are summarized in Table 1. Glycopeptides in peak T3 can be identified as a mixture of peptide His21-His31 and His21-Glu32 glycosylated at Asn23, and Ser96-Asp106 glycosylated at Asn98. Asn23 was attached by high-mannose-type oligosaccharides, M5, 6, and 7, and Asn98 was occupied by *N*-glycan consisting of $dHex_1Hex_4HexNAc_4$ with a Lewis a/x structure as a partial structure. Glycopeptides in peak T5 were characterized as peptide His21-Phe33 glycosylated at Asn23 with high-mannose-type oligosaccharide, M6. Glycopeptides in peak T7 were assigned to be Val69-Lys78 glycosylated at Asn74 with *N*-glycans composed of $dHex_{1-2}Hex_{4-6}HexNAc_{3-6}NeuAc$.

3.4. Analysis of the GPI moiety of rat Thy-1

Since trypsin digestion provided Cys-GPI, which could not be retained on the C_{18} column, Asp-N digestion was also performed to obtain more hydrophobic peptides attached by GPI (GPI-peptides). Fig. 6(A) shows the peptide/glycopeptide map obtained by LC/ITMS of Asp-N digested Thy-1. We localize the GPI-peptides using marker ions, EtN-PO_4-Man^+ at *m/z* 286 and GlcN-inositol-PO_4^+ at *m/z* 422, originating from the core structure of the GPI moiety by in-source CID (EtN, ethanolamine; GlcN, glucosamine). Mass chromatograms of *m/z* 286 and 422 suggest the locations of the GPI-peptides to be around 4.2 (peak A1-1) and 4.4 min (peak A1-2) (Fig. 6(B and C)). Using product ions originated from GPI moiety, such as GlcN-inositol-PO_4^+ and PO_4-Man-$GlcN^+$ (*m/z* 422 and 404), as marker ions, four product ion spectra of GPI-peptides were sorted out from all product ion spectra around peaks A1-1 and 1-2. Their precursor ions were doubly charged ions at *m/z* 1132 and 1213 (peak A1-1), 1051 and 1151 (peak A1-2). Based on these product ion spectra, we characterized GPI-peptides as the peptide Asp106-Cys111 with a GPI core structure plus Hex_{0-2}, $HexNAc_{1-2}$ and PO_4-EtN.

Fig. 7(A) shows the product ion spectrum of the doubly charged GPI-peptide ion at *m/z* 1051 in peak A1-2. In addition to product ions at *m/z* 422, those originating from the GPI moiety were detected at *m/z* 404 (PO_4-Man-$GlcN^+$), 447 (EtN-PO_4-Man-$GlcN^+$), 650 (EtN-PO_4-(HexNAc-)Man-$GlcN^+$), 787 (peptide-EtN^+), 868 (peptide-EtN-PO_4^+), 1191 (peptide-EtN-PO_4-Man-Man^+), 1477 (peptide-EtN-PO_4-Man-Man-(EtN-PO_4-)Man^+), 1638 (peptide-EtN-PO_4-Man-Man-(EtN-PO_4-)Man-$GlcN^+$), and 1898 (peptide-EtN-PO_4-Man-Man-(EtN-PO_4-)Man-GlcN-inositol-PO_4^+). From these fragments, it can be deduced that this peptide is Asp106-Cys111 carrying the GPI, as indicated in the inset in Fig. 7(A).

The other GPI-peptide in peak A1-1 was characterized as having side chains; -Hex attached to M1, -PO_4-EtN and -HexNAc attached to M3, based on the product ion spectrum of the doubly charged precursor ion at *m/z* 1132 (data not shown). These two GPI structures are identical to those that have been previously reported [24].

Product ion spectra of doubly charged ion at *m/z* 1151 and 1213 suggested that they contained GPI which bear one HexNAc or two Hex in addition to GPI in Fig. 7(A) respectively. Fig. 7(B) shows the product ion spectra of the doubly charged precursor ions at *m/z* 1151 in peak A1-2. In addition to *m/z* 422, we detected product ions at *m/z* 366 (HexNAc-Man^+), 447 (EtN-PO_4-Man-$GlcN^+$), 650 (EtN-PO_4-(HexNAc-)Man-$GlcN^+$), 1229 (peptide-EtN-PO_4-(HexNAc-)Man^+), 1391 (peptide-EtN-PO_4-(HexNAc-)Man-Man^+), 1676 (peptide-EtN-PO_4-(HexNAc-)Man-Man-(EtN-PO_4-)Man^+), 1838 (peptide-EtN-PO_4-(HexNAc-)Man-Man-(EtN-PO_4-)Man-$GlcN^+$), and 1880 (peptide-EtN-PO_4-(HexNAc-)Man-Man-(EtN-PO_4-)(HexNAc-)Man^+). These fragment ions suggest the attachment of -HexNAc to Man1, and -PO_4-EtN and -HexNAc to Man3 as indicated in the inset of Fig. 7(B). Similarly, product ion spectra of the doubly charged precursor ion at *m/z* 1213 indicate the attachment of 2Hex and HexNAc to Man1 and Man3-PO_4-EtN (data not shown). To our knowledge, this is the first report of these two GPI structures in Thy-1.

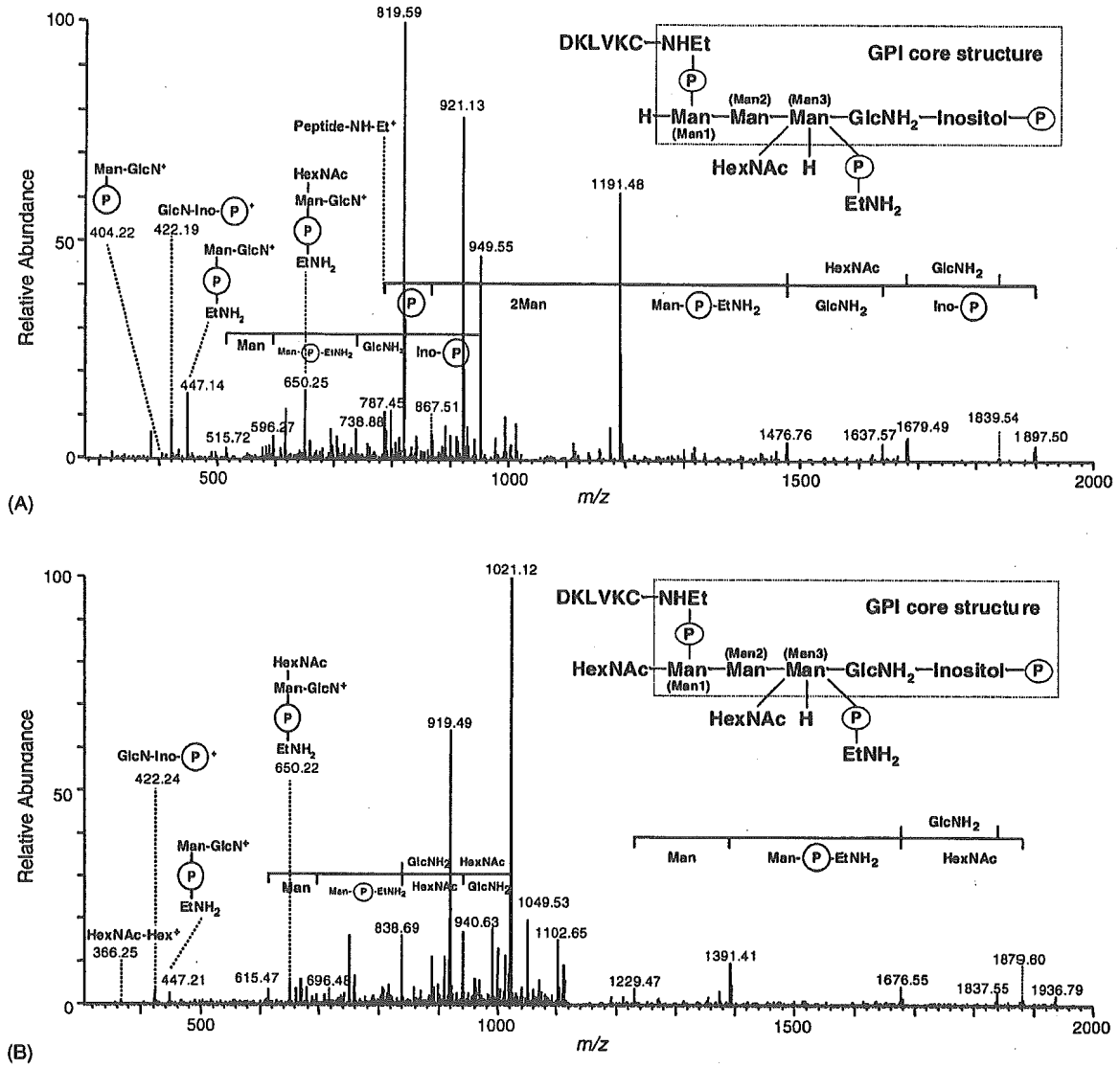

Fig. 7. Product ion spectra of the doubly charged GPI-peptide at *m/z* 1051 (A), and at *m/z* 1151 (B) in peak A1-2. The inset is the deduced structure of the GPI-peptide, and the core structure of GPI is the inside dashed line. Man, mannose; HexNAc, *N*-acetylhexosamine; $GlcNH_2$, glucosamine; $EtNH_2$-P, phosphorylethanolamine; Ino-P, inositol-phosphate.

3.5. Analysis of Asp-N digested Thy-1

Glycopeptides obtained by Asp-N digestion were also localized by in-source CID using marker ions at *m/z* 204 and 292 (Fig. 6(D and E)), and neutral loss of 81 u by data-dependent CID-MS/MS (Fig. 6(F)). Product ion spectra of glycopeptides were sorted by using B series ions as marker ions from those acquired around localized elution positions. Consequently, peaks A2-7 were identified as those of glycopeptides (Fig. 6(A)). The oligosaccharide structures in the glycopeptides were then characterized based on their product ion spectra (Table 1). In addition to the high-mannose-type oligosaccharides, M5, 6, and 7 deduced by LC/MS^n of tryptic digests, the oligosaccharide at Asn23 was characterized as $dHex_{0-1}Hex_{3,5,6}HexNAc_{3-5}NeuAc_{0,1}$, complex-type and hybrid-type oligosaccharides containing Lewis a/x or bisecting GlcNAc as a partial structure. Asn74 is attached by *N*-glycans with $dHex_{0-2}Hex_{3-6}HexNAc_{2,4,5}NeuAc_{0,1}$. They were high-mannose-type oligosaccharide, M5, complex-type oligosaccharides containing core Fuc and Lewis a/x as a partial structure, and hybrid-type oligosaccharides with core Fuc. Asn98 is occupied by high-mannose-type oligosaccharides, M5, and *N*-glycans with $dHex_{0-2}Hex_{3,5,6}HexNAc_{2-5}NeuAc_{0,1}$, hybrid-type oligosaccharides containing Lewis a/x or blood group H-determinant as a partial structure, which were found to be of greater diversity than those deduced by analysis of tryptic digests.

4. Discussion

In the present study, we have developed an efficient and convenient strategy for characterization, including protein identification and glycosylation analysis, of a small amount of unknown protein. We used gel electrophoresis, which is a powerful tool for separation of a small amount of protein from complex proteins mixture, especially from insoluble membrane fractions. For the complete glycosylation analysis, we examined the extraction of a whole glycoprotein from the gel, followed by trypsin digestion. Additionally, for the effective glycopeptide analysis, we studied mass spectrometric peptide/glycopeptide mapping by LC/MS^n with in-source CID and data-dependent MS^n. The glycopeptides were localized in the peptide/glycopeptide map by using oxonium ions as marker ions such as $HexNAc^+$ and $NeuAc^+$, which were generated by in-source CID, and neutral loss by data-dependent CID-MS/MS. For simultaneous identification of both peptides and glycopeptides, we conducted the database search analysis using search parameters containing a possible glycosylation at Asn with GlcNAc (203 Da). We successfully determined the sequences of peptides and some of the glycopeptides, which were localized by in-source CID and data-dependent CID-MS^n. The database search analysis using these search parameters was useful for identifying the glycopeptides resulting from predictable proteinase digestion. Glycopeptides caused by irregular digestion could be identified by assignment of peptide b and y series ions, which arose from further MS^n. The oligosaccharide structures of the identified glycopeptides were characterized on the basis of their product ion spectra. In this way, we were able to isolate rat brain Thy-1 and to elucidate *N*-glycosylation at Asn23, 74, and 98 as well as the structure of the GPIs at Cys111.

Post-translationally modified peptides could not be identified by the database search analysis. It has been particularly difficult to identify glycopeptides by database search analysis due to their complicated product ions resulting from the cleavage of glycosidic bonds. It has recently been reported that peptide + GlcNAc ion generated from a glycopeptide by CID-MS/MS yields b and y series ions by further MS^n, and that these ions can be utilized for identification of the peptide backbone and its glycosylation site [15,16,18]. Additionally, search analysis using the database including the possibility of glycosylation at Asn with all possible cleavage products of the known glycopeptides can be utilized for identification of glycopeptides in the peptide/glycopeptide map [19]. This ability would be helpful in the identification of glycoproteins whose glycosylation are already known. In the present study, we carried out a database search analysis using search parameters containing a possible glycosylation at Asn with only GlcNAc (203 Da), and successfully identified an unknown glycoprotein and *N*-glycosylated sites. This search analysis can be used for the identification of *O*-glycosylation, which has no consensus amino acid sequence, by using search parameters containing possible glycosylations at Ser/Thr with Hex, HexNAc, and dHex.

Precursor ion scans have been used for the localization the glycopeptides in peptide/glycopeptide mapping [10,11,13]. Although this method can be used for monitoring the peptides with predictable modification by setting mass of fragment ions prior to scanning, peptides with unpredictable modification cannot be detected. In contrast, in-source CID and CID-MS/MS are capable of localizing of the modified peptides after just one data acquisition using objective oxonium ions and neutral losses. In the present study, we were able to localize GPI-peptides in the peptide/glycopeptide map using EtN-PO_4-Man^+ and GlcN-Inositol-PO_4^+ generated by in-source CID [25] and to elucidate the GPI structures. We also could localize the glycopeptides with dHex, HexNAc, and NeuAc at the non-reducing ends as well as Hex using neutral loss by CID-MS/MS.

Site-specific glycosylation analysis of rat brain Thy-1 was performed after purification with monoclonal antibody affinity chromatography. Released oligosaccharides from fractionated trypsin-digested glycopeptides were analyzed by conventional analytical methods, including exoglycosidase digestion and methylation analysis [26]. In the present study, we separated PIPLC-treated GPI-anchored proteins of rat brain by SDS-PAGE, and conducted site-specific glycosylation analysis by LC/MS^n. Using a simpler step, we could elucidate the glycosylation at each glycosylation site with a greater variety of oligosaccharides than that reported previously and four GPI structures, including two novel attached structures.

Our strategy presented herein can relatively simply facilitate complete site-specific glycosylation analysis that used to require a series of complicated steps and is applicable to characterization of unknown proteins on 2-DE gel in proteomic study. Even in a mixture of multiple unknown glycoproteins, glycosylation of each glycoprotein can be determined based on the product ion spectra. Our method would be helpful for study of the alternation of glycosylation with growth, aging, and disease [27,28].

Acknowledgements

This study was supported in part by a Grant-in-Aid from the Ministry of Health, Labor and Welfare, Core Research for the Evolutional Science and Technology Program (CREST) of the Japan Science and Technology Agency (JST), and Research on Health Science focusing on Drug Innovation from The Japan Health Science Foundation (N.K.).

We appreciate Dr. A. Hachisuka of the National Institute of Health Science for her technical advice.

We would also like to thank Dr. M. Kubota and Mr. M. Yoshida of Thermo Electron K.K. (Japan), for their technical support.

References

[1] A. Varki, Glycobiology 3 (1993) 97.
[2] H. Sasaki, B. Bothner, A. Dell, M. Fukuda, J. Biol. Chem. 262 (1987) 12059.
[3] F. Wang, A. Nakouzi, R.H. Angeletti, A. Casadevall, Anal. Biochem. 314 (2003) 266.
[4] K. Hirayama, R. Yuji, N. Yamada, K. Kato, Y. Arata, I. Shimada, Anal. Chem. 70 (1998) 2718.
[5] M. Ohta, N. Kawasaki, S. Itoh, T. Hayakawa, Biologicals 30 (2002) 235.
[6] E. Mortz, T. Sareneva, S. Haebel, I. Julkunen, P. Roepstorff, Electrophoresis 17 (1996) 925.
[7] F.G. Hanisch, M. Jovanovic, J. Peter-Katalinic, Anal. Biochem. 290 (2001) 47.
[8] D. von Witzendorff, M. Ekhlasi-Hundrieser, Z. Dostalova, M. Resch, D. Rath, H.W. Michelmann, E. Topfer-Petersen, Glycobiology 15 (2005) 475.
[9] B. Küster, T.N. Krogh, E. Mortz, D.J. Harvey, Proteomics 1 (2001) 350.
[10] S.A. Carr, M.J. Huddleston, M.F. Bean, Protein Sci. 2 (1993) 183.
[11] M.J. Huddleston, M.F. Bean, S.A. Carr, Anal. Chem. 65 (1993) 877.
[12] R.S. Annan, S.A. Carr, J. Protein Chem. 16 (1997) 391.
[13] K. Sandra, I. Stals, P. Sandra, M. Claeyssens, J. Van Beeumen, B. Devreese, J. Chromatogr. A 1058 (2004) 263.
[14] A. Harazono, N. Kawasaki, T. Kawanishi, T. Hayakawa, Glycobiology 15 (2005) 447.
[15] U.M. Demelbauer, M. Zehl, A. Plematl, G. Allmaier, A. Rizzi, Rapid Commun. Mass Spectrom. 18 (2004) 1575.
[16] Y. Wada, M. Tajiri, S. Yoshida, Anal. Chem. 76 (2004) 6560.
[17] B. Sullivan, T.A. Addona, S.A. Carr, Anal. Chem. 76 (2004) 3112.
[18] S. Zhang, D. Chelius, J. Biomol. Tech. 15 (2004) 120.
[19] S. Wu, P. Bondarenko, T. Shaler, P. Shieh, W. Hancock, Thermo Finnigan LC/MS^n Application Report Application Report No. 300.
[20] C. Bordier, J. Biol. Chem. 256 (1981) 1604.
[21] M.P. Lisanti, M. Sargiacomo, L. Graeve, A.R. Saltiel, E. Rodriguez-Boulan, Proc. Natl. Acad. Sci. U.S.A. 85 (1988) 9557.
[22] S. Itoh, N. Kawasaki, M. Ohta, T. Hayakawa, J. Chromatogr. A 978 (2002) 141.
[23] B. Domon, C.E. Costello, J. Glycoconjugate 5 (1988) 397.
[24] S.W. Homans, M.A. Ferguson, R.A. Dwek, T.W. Rademacher, R. Anand, A.F. Williams, Nature 333 (1988) 269.
[25] K. Fukushima, Y. Ikehara, M. Kanai, N. Kochibe, M. Kuroki, K. Yamashita, J. Biol. Chem. 278 (2003) 36296.
[26] R.B. Parekh, A.G. Tse, R.A. Dwek, A.F. Williams, T.W. Rademacher, EMBO J. 6 (1987) 1233.
[27] Y. Sato, M. Kimura, C. Yasuda, Y. Nakano, M. Tomita, A. Kobata, T. Endo, Glycobiology 9 (1999) 655.
[28] G. Durand, N. Seta, Clin. Chem. 46 (2000) 795.

Available online at www.sciencedirect.com
SCIENCE DIRECT®
Journal of Chromatography A, 1103 (2006) 296–306
JOURNAL OF CHROMATOGRAPHY A
www.elsevier.com/locate/chroma

N-linked oligosaccharide analysis of rat brain Thy-1 by liquid chromatography with graphitized carbon column/ion trap-Fourier transform ion cyclotron resonance mass spectrometry in positive and negative ion modes

Satsuki Itoh[a], Nana Kawasaki[a,b,*], Noritaka Hashii[b], Akira Harazono[a], Yukari Matsuishi[a], Takao Hayakawa[c], Toru Kawanishi[a]

[a] *Division of Biological Chemistry and Biologicals, National Institute of Health Science, 1-18-1 Kamiyoga, Setagaya-ku, Tokyo 158-8501, Japan*
[b] *CREST, Japan Science and Technology Agency (JST), Japan*
[c] *Pharmaceutical and Medical Devices Agency, 3-3-2 Kasumigaseki, Chiyoda-ku, Tokyo 100-0013, Japan*

Received 25 July 2005; received in revised form 10 November 2005; accepted 14 November 2005
Available online 20 December 2005

Abstract

We have previously described the site-specific glycosylation analysis of rat brain Thy-1 by LC/multistage tandem mass spectrometry (MS^n) using proteinase-digested Thy-1. In the present study, detailed structures of oligosaccharides released from Thy-1 were elucidated by mass spectrometric oligosaccharide profiling using LC/MS with a graphitized carbon column (GCC–LC/MS). First, using model oligosaccharides, we improved the oligosaccharide profiling by ion trap mass spectrometry (IT–MS) coupled with Fourier transform ion cyclotron resonance mass spectrometry (FT–ICR–MS). Sequential scanning of a full MS^1 scan with FT–ICR–MS followed by data-dependent MS^n with IT–MS in positive ion mode, and a subsequent full MS^1 scan with FT–ICR–MS followed by data-dependent MS^n with IT–MS in negative ion mode enabled the monosaccharide composition analysis as well as profiling and sequencing of both neutral and acidic oligosaccharides in a single analysis. The improved oligosaccharide profiling was applied to elucidation of N-linked oligosaccharides from Thy-1 isolated by sodium dodecyl sulfate-polyacrylamide gel electrophoresis. It was demonstrated that Thy-1 possesses a significant variety of N-linked oligosaccharides, including Lewis a/x, Lewis b/y, and disialylated structure as a partial structure. Our method could be applicable to analysis of a small abundance of glycoproteins, and could become a powerful tool for glycoproteomics.

Keywords: Mass spectrometric oligosaccharide profiling; Graphitized carbon column; Ion trap mass spectrometry; Fourier transform ion cyclotron resonance mass spectrometry; Data-dependent MS^n; Thy-1

1. Introduction

Glycosylation is one of the most abundant post-translational modifications of proteins [1]. It is already known that glycosylation influences the biological functions as well as the physicochemical properties of proteins, i.e., folding, solubility, aggregation, and stability. A number of reports have noted a positive relationship between a change in glycosylation and development, aging, and certain diseases [2–4]. Elucidation of structural detail in oligosaccharides is necessary to clarify the biological properties of glycoproteins.

MS is now a powerful tool for structural analysis of glycoproteins. There are two major mass spectrometric approaches to the structural analysis of glycoproteins, i.e., MS of glycopeptides [5–7] and of oligosaccharides [8–13]. For oligosaccharide sequencing, tandem mass spectrometry as well as exoglycosidase digestions in conjuction with MS is recognized as an effective means of oligosaccharide sequencing [14–16]. Mass spectrometric peptide/glycopeptide mapping by LC coupled with tandem mass spectrometry (LC/MS/MS) is effective for the determination of glycosylation sites and the analysis of site-specific heterogeneity [17–22]. However, structural detail in

* Corresponding author. Division of Biological Chemistry and Biologicals, National Institute of Health Science, 1-18-1, Kamiyoga, Setagaya-ku, Tokyo 158-8501, Japan. Tel.: +81 3 3700 1141; fax: +81 3 3707 6950.
E-mail address: nana@nihs.go.jp (N. Kawasaki).

0021-9673/$ – see front matter © 2005 Elsevier B.V. All rights reserved.
doi:10.1016/j.chroma.2005.11.043

oligosaccharides is not always available by product ion spectra of glycopeptides, as many of the precursor ions consist of uniform peptides carrying different oligosaccharides with identical *m/z* values. LC/MS/MS of glycopeptides has limitations for the structural analysis of carbohydrates due to the difficulty of isolating of glycopeptide isomers. Mass spectrometric oligosaccharide profiling through the separation of isomers by LC can supply the structural detail of each oligosaccharide although it cannot provide information regarding glycosylation sites and site-specific glycosylation [23–29]. MS of both glycopeptides and oligosaccharides is needed for glycosylation analysis of a glycoprotein [30].

Thy-1 is a cell adhesion molecule that belongs to the immunoglobulin superfamily and is attached to the cell membrane via a glycosylphosphatidylinositol (GPI)-anchor. We recently, studied the glycosylation of Thy-1 in rat brain by mass spectrometric peptide/glycopeptide mapping, and demonstrated that Thy-1 possesses various *N*-glycans at Asn23, 74, and 98 [31]. The monosaccharide composition of *N*-glycan at each glycosylation site was estimated by masses of molecular ions; however, structural detail regarding some of the oligosaccharides could not be elucidated by MS^n since many glycopeptides with identical *m/z* values contained several oligosaccharide isomers and yielded product ions from a mixture of these glycopeptide isomers. Mass spectrometric oligosaccharide profiling is necessary for detailed structural analysis of oligosaccharides.

We have previously demonstrated a simple means of oligosaccharide profiling using liquid chromatography/electrospray ionization mass spectrometry with a graphitized carbon column (GCC–LC/MS) [32–34], in which oligosaccharides can be separated on the basis of their branching, sequence, and linkage, and can be characterized based on their monosaccharide compositions estimated from their calculated molecular masses. Here, we study the glycosylation of Thy-1 by oligosaccharide profiling with GCC–LC/MS. First, we improved our oligosaccharide profiling by ion trap mass spectrometry (IT–MS) coupled with Fourier transform ion cyclotron resonance mass spectrometry (FT–ICR–MS). This instrument is capable of both monosaccharide composition analysis by acquisition of accurate masses and data-dependent multistage tandem MS (MS^n) for sequencing with fast switching between positive and negative ion modes. Using a mixture of typical oligosaccharides, including high-mannose-type, and asialo-, trisialylated, and tetrasialylated complex-types, we confirmed that the improved method can be used for monosaccharide composition analysis and detailed structural analysis of both neutral and acidic oligosaccharides. The method was then applied to N-linked oligosaccharide analysis of rat brain Thy-1.

2. Experimental

2.1. Materials

Man7/D1, Man7/D3, and asialo-triantennary (Tri) were obtained from Oxford Glycosystems (Abingdon, UK). Trisialylated triantennary ($TriNA_3$) and tetrasialylated tetraantennary ($TetraNA_4$) were purchased from Dionex (Sunnyvale, CA, USA). Rat brain was purchased from Nippon SLC (Hamamatsu, Japan). Phosphatidylinositol-specific phospholipase C (PIPLC) from *Bacillus cereus* was purchased from Molecular Probes (Eugene, OR, USA). Peptide-*N*-glycosidase F (PNGase F) was purchased from Roche Diagnostics (Mannheim, Germany). SimplyBlue SafeStain was obtained from Invitrogen (Carlsbad, CA, USA).

2.2. Release of N-linked oligosaccharides from rat brain Thy-1 by in-gel PNGase F digestion

PIPLC-treated GPI-anchored proteins were prepared from rat brain as reported previously [31]. Briefly, the homogenate of rat brain was defatted and solubilized with 2% Triton X-114 at 4 °C overnight [35,36]. After centrifugation, the supernatant was subjected to Triton X-114 phase-partitioning at 37 °C. Solubilized membrane proteins in the detergent phase were precipitated with cold acetone, and the precipitates were digested with PIPLC. After resubjecting the digest mixture to Triton X-114 phase-partitioning, PIPLC-treated soluble GPI-anchored proteins in aqueous phase were precipitated by adding cold acetone. These proteins were carboxyamidomethylated [30], and were separated by sodium dodecyl sulfate–polyacrylamide gel electrophoresis (SDS–PAGE) (12.5%) followed by staining with SimplyBlue SafeStain.

In-gel PNGase F digestion of Thy-1 and extraction of N-linked oligosaccharides were performed as previously described

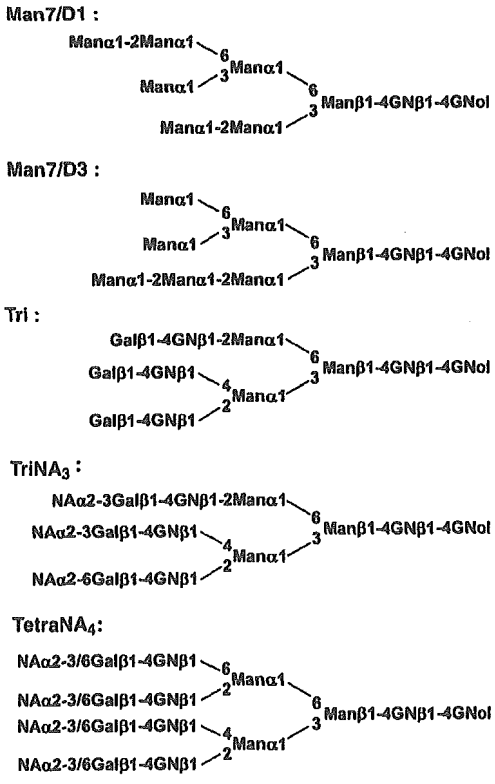

Fig. 1. Structures of major oligosaccharides and their abbreviations. Man: mannose, Gal: galactose, GN; *N*-acetylglucosamine, GNol; *N*-acetylglucosaminitol, NA; *N*-acetylneuramic acid.

[15]. The protein band of Thy-1 (20–25 kDa) was excised, cut into pieces, and destained. The gel pieces were dehydrated with 50% acetonitrile. The dried gels were then equilibrated with 50 mM sodium phosphate buffer (pH 7.2) and incubated at 37 °C with 3 units of PNGase F. The released *N*-glycans were extracted three times from gel pieces by intermittent sonication for 30 min in water. All extracts were combined and lyophilized. The released N-linked oligosaccharides were reduced with $NaBH_4$, as previously reported [33], and subjected to GCC–LC/IT–MS-FT–ICR–MS.

2.3. *N-linked oligosaccharide analysis by GCC–LC/IT–MS-FT–ICR–MS*

GCC–LC/MS was carried out using a MAGIC 2002 system (Michrom BioResource, Auburn, CA, USA) connected to IT–MS instrument coupled with FT–ICR–MS instrument (Finnigan LTQ FT, Thermo Electron Corp., San Jose, CA, USA). The eluents consisted of 5 mM ammonium acetate, pH 9.6, containing 2% CH_3CN (pump A), and 5 mM ammonium acetate, pH 9.6, containing 80% CH_3CN (pump B). The borohydride-reduced N-linked oligosaccharides were separated on Hypercarb (150 mm × 0.2 mm, 5 μm, Thermo Electron Corp.) as GCC with a linear gradient of 5–30% for pump B over a period of 60 min at a flow rate of 2 μl/min.

The MS^n experiment includes sequential scans, as follows: a full MS^1 scan (*m/z* 700–2000) by FT–ICR–MS in positive ion mode, data-dependent MS^n scans by IT–MS for most abundant ions regardless of their charge state, a full MS^1 scan (*m/z* 700–2000) by FT–ICR–MS in negative ion mode, and data-dependent MS^n scans by IT–MS for the most intense ions regardless of their charge state. For the data-dependent MS^n, the following settings were used: the isolation window for precursor masses, ±2.5 Da; collision energy, 35%; dynamic exclusion

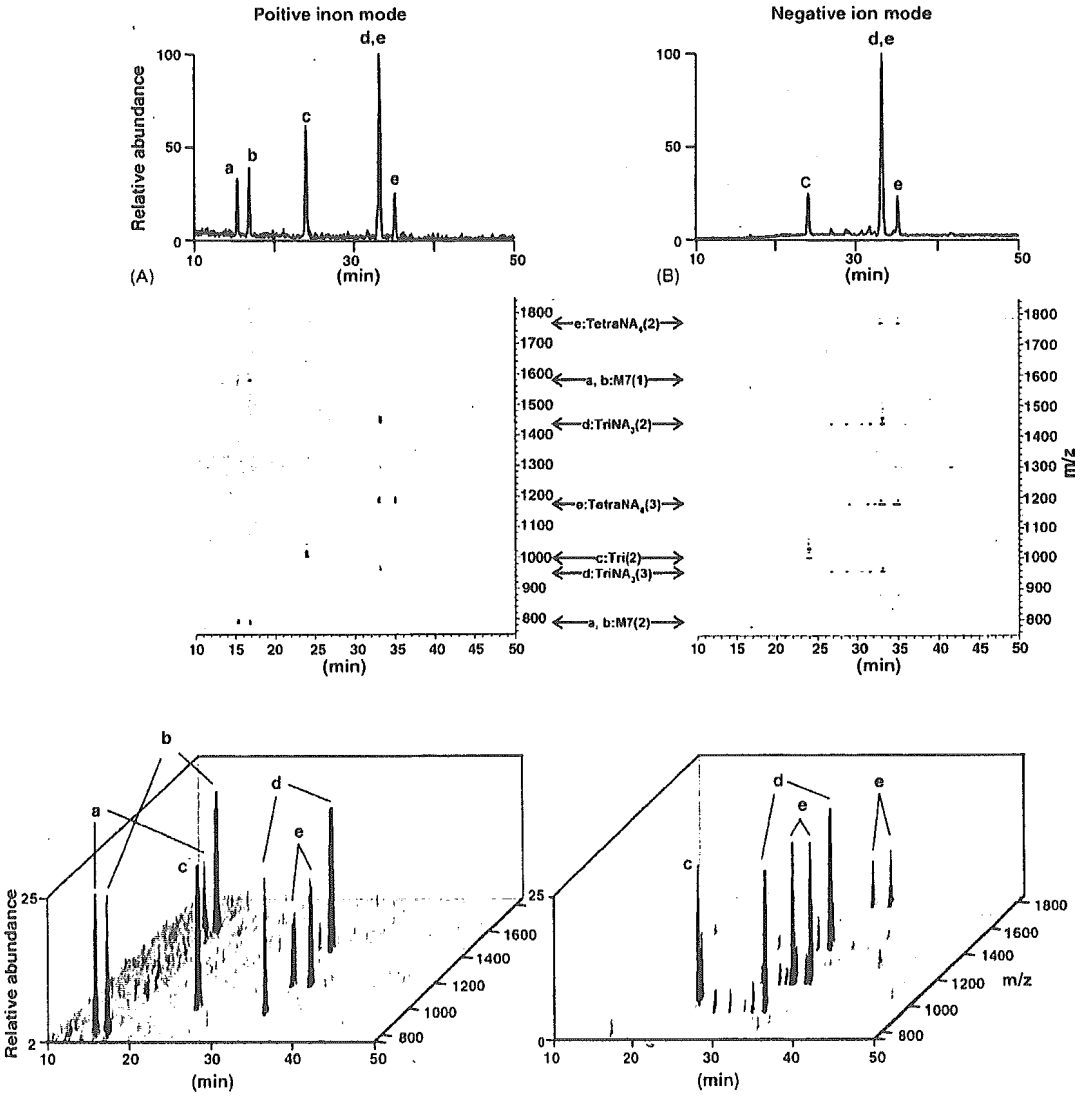

Fig. 2. Typical oligosaccharide profiles obtained by full MS^1 scans with FT–ICR–MS. (A) total ion chromatogram (TIC) (upper), two-dimensional (2D) display (retention time vs. *m/z*) (middle), and three-dimensional (3D) display (lower) in positive ion mode. (B) TIC (upper), 2D (middle) and 3D display (lower) in negative ion mode. Numbers in parentheses after the abbreviation of the model oligosaccharides refer to the charge state.

time, 15 s. The operating conditions employed for LC/MS^n were as follows: tube lens offset, 120 V; capillary voltage, 2.0 kV; and capillary temperature, 200 °C.

3. Results

3.1. GCC–LC/IT–MS-FT–ICR–MS of model oligosaccharides

By using the IT–MS-FT–ICR–MS instrument, the oligosaccharide profiling was shown to be more rapid, accurate, and informative. Man7/D1, Man7/D3, Tri, $TriNA_3$, and $TetraNA_4$, which were chosen as model neutral and acidic oligosaccharides (Fig. 1), were analyzed by alternative scans in positive and negative ion modes, which are consisting of a full MS^1 scan by FT–ICR–MS followed by data-dependent MS^n scans by IT–MS. Fig. 2A and B show the oligosaccharide profiles obtained by a full MS^1 scan with FT–ICR–MS (*m/z* 700–2000) in positive and negative ion modes, respectively. The monosaccharide compositions of individual oligosaccharides could be easily determined by accurate *m/z* values, and the major peaks of a, b, c, d, and e were assigned to Man7/D1 or D3, Man7/D3 or D1, Tri, $TriNA_3$ and $TetraNA_4$, respectively. Oligosaccharides detected at the same *m/z* values are positional isomers. Man7/D1 and D3 were detected in positive ion mode, but were only slightly detectable in negative ion mode. The major isomers of $TriNA_3$ and $TetraNA_4$ were detected in both ion modes, whereas their minor isomers were detected only in negative ion mode. These results demonstrate the advantage of alternative scans in both ion modes.

We confirmed the possibility of data-dependent MS^n scans for sequencing neutral and sialylated oligosaccharides. Man 7/D1 and D3 could be distinguished from each other by data-dependent MS^n (Fig. 3). Oligosaccharide eluted at 15 min could be assigned to Man7/D1 by the relatively intense ions at *m/z* 913 ($Y_{3\alpha}^+$) and 1237 ($Y_{3\beta}^+$), which would be predominantly produced from Man7/D1 by the cleavage of the α1–6-linked or α1–3-linked branch arm of the core mannose (Fig. 3A) (nomenclature proposed by Domon and Costello [37]). Likewise, the oligosaccharide at 17 min could be Man7/D3 based on the intensity of Y_{3x}^+ at *m/z* 1075 generated from Man7/D3 by the cleavages of both the α1–6-linked and α1–3-linked branch arms (Fig. 3B).

Fig. 4A and B show the product ion spectra of $TetraNA_4$ in positive and negative ion modes, respectively. In positive ion mode, the characteristic B ions such as *m/z* 454 (B_{2x}^+), 657 (B_{3x}^+), 1475 (B_{4x}^+), and 1658 (B_6^{2+}), and a ladder of several Y ions with intervals corresponding to Hex, HexNAc, and NeuAc were detected. B/Y ions were also detected at *m/z* 366, 527, 819 (B_5/Y_{3x}^{2+}), and 1330 (B_6/Y_{4x}^{2+}). In negative ion mode, only sialic acids were predominantly eliminated by MS^2 and MS^3. The structural information was provided by MS^4, whereby both B and Y ions were originated from $TetraNA_2$, together with the internal fragmentation ions and cross ring cleaved ions (Fig. 4B). In addition to the B and Y ions, which were predominantly produced in positive ion mode, fragment ions at *m/z* 470 ($C_{2x'}^-$), 1322 ($Z_{6x'}^{2-}$, $[Y_{6x'}\text{-}H_2O]^{2-}$), 1241 ($Z_{5x'}^{2-}$, $[Y_{5x'}\text{-}H_2O]^{2-}$), and 1057 ($Y_{5x''}/Z_{4x'}^{2-}$, $Y_{4x'}/Z_{5x''}^{2-}$, $Y_{4x''}/Z_{5x'}^{2-}$, $Y_{5x'}/Z_{4x''}^{2-}$, $[Y_{4x'/5x''}\text{-}H_2O]^{2-}$, $[Y_{4x''/5x'}\text{-}H_2O]^{2-}$) were detected in negative ion mode. These ions were also useful for the structural characterization of oligosaccharides.

3.2. Glycosylation analysis of Thy-1 by GCC–LC/IT–MS-FT–ICR–MS

The improved oligosaccharide profiling using IT–MS-FT–ICR–MS was applied to the glycosylation analysis of Thy-1. PIPLC-treated Thy-1 in rat brain was isolated by SDS–PAGE [31]. N-linked oligosaccharides were extracted from the gel after in-gel PNGase F digestion and were reduced

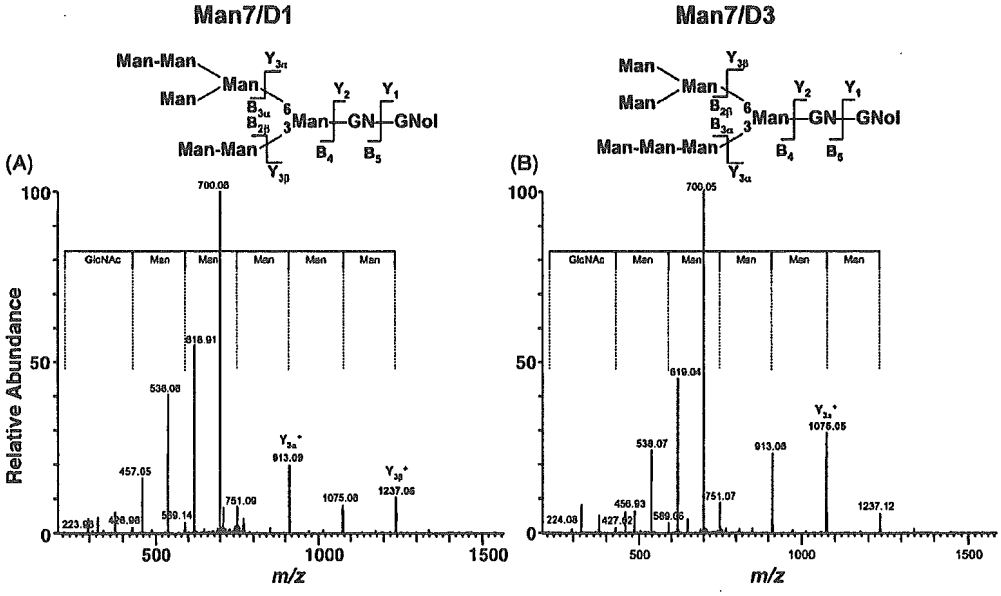

Fig. 3. Product ion spectra of oligosaccharide Man 7/D1 (A) and Man 7/D3 (B).

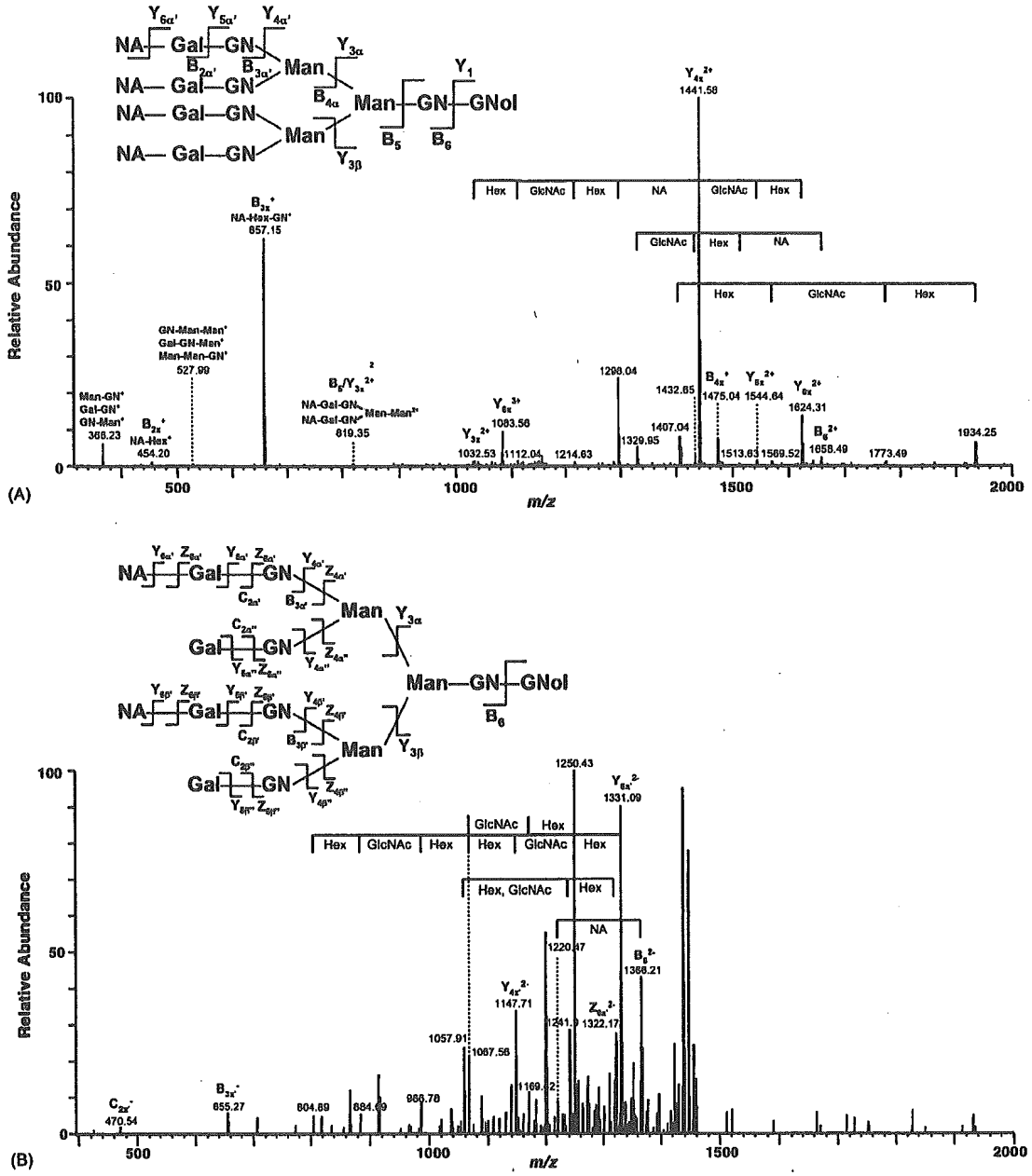

Fig. 4. Product ion spectra of model oligosaccharide, TetraNA$_4$. (A) MS^2 spectrum derived from $[TetraNA_4]^{3+}$ at *m/z* 1180 in positive ion mode. (B) MS^4 spectrum derived from $[TetraNA_4]^{3-}$ at *m/z* 1178 → $[TetraNA_3]^{3-}$ at *m/z* 1081 → $[TetraNA_2]^{2-}$ at *m/z* 1476 in negative ion mode.

with $NaBH_4$. Fig. 5 shows total ion chromatogram (TIC) (A) obtained by GCC–LC/IT–MS-FT–ICR–MS of borohydrate-reduced oligosaccharides, and two-dimensional display of full MS^1 scans in positive ion mode (red) and negative ion mode (blue) (B), in which oligosaccharides appear as protonated and ammonium adducted forms along with fragment ions. Alternative scanning in potitive and negative ion mode enables us to detect many oligosaccharides without missing less ionized oligosaccharides in either ion mode. For example, oligosaccharides at *m/z* 762 (2+) and 822 (2+) were detected only in positive ion mode, whereas those at *m/z* 1387 (2−), 1440 (2−), and 1542 (2−) were detected only in negative ion mode. Furthermore, accurate *m/z* values acquired by FT–ICR–MS provide their monosaccharide composition, and subsequent data-dependent MS^n allows us to elucidate their monosaccharide sequence as follows.

3.2.1. Monosaccharide composition of oligosaccharides

Oligosaccharides in Thy-1 were assigned to $NeuAc_{0-3}$ $dHex_{0-3}Hex_{3-9}HexNAc_{1-5}HexNAcol_1$ based on their accurate *m/z* values (Table 1). Oligosaccharides bearing two Fuc residues, in which the *m/z* values of multiple charged ions are nearly identical to those of oligosaccharides bearing one NeuAc residue instead, could be determined

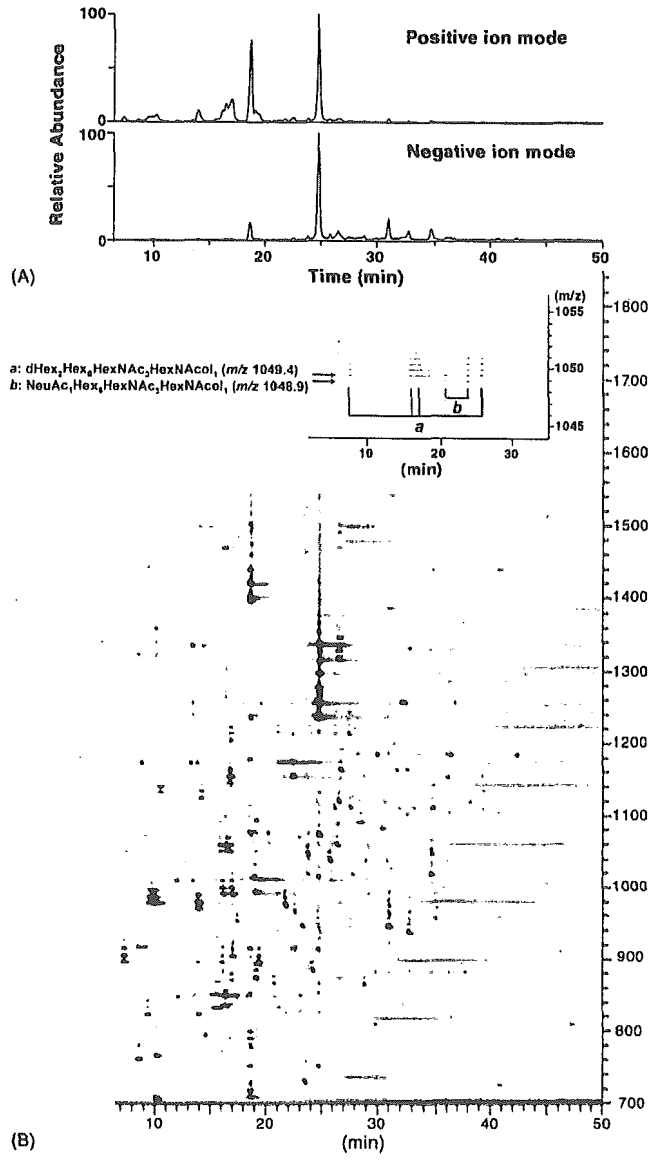

Fig. 5. N-Linked oligosaccharide profile of rat brain Thy-1 obtained by full MS^1 scans with FT–ICR–MS. (A) TIC, and (B) overlapped 2D display in positive (red) and negative (blue) ion modes.

by FT–ICR–MS. For instance, difucosylated oligosaccharides ($dHex_2Hex_6HexNAc_3HexNAcol_1$, theoretical molecular weight: 2096.78 Da) detected at 7.6, 16, 17, and 26 min (Fig. 5, inset, a) were clearly distinguished from monosialylated oligosaccharides ($NeuAc_1Hex_6HexNAc_3HexNAcol_1$, theoretical molecular weight: 2095.76 Da) detected at 21 and 24 min (Fig. 5, inset, b). The improved oligosaccharide profiling indicated that Thy-1 possesses a significant variety of N-linked oligosaccharides containing high-mannose-type (Man5, Man6, Man7, Man8, and M9) and many different complex- and hybrid-type oligosaccharides bearing $NeuAc_{0-3}$ and Fuc_{0-3}. These results are coincident with those of our previous study, in which we carried out mass spectrometric analysis of Thy-1 glycopeptides.

3.2.2. Monosaccharide sequence of oligosaccharides

Monosaccharide sequences of oligosaccharides were elucidated based on the MS/MS spectra. One of the remarkable features of Thy-1 oligosaccharides is the attachment of multiple Fuc and NeuAc residues. We describe below some examples of assignment fucosylated and sialylated oligosaccharides.

3.2.2.1. Gal-(Fuc–)GlcNAc–(Lewis a/x type). Fig. 6A shows the product ion spectrum of a difucosylated oligosaccharide, $dHex_2Hex_4HexNAc_3HexNAcol_1$, at *m/z* 887 (24.3 min) in positive ion mode. There are two possible sites of fucosylation: GlcNAc at the non-reducing end and at the reducing end in the trimannosyl core. The ions detected at *m/z* 350 (Fuc-GlcNAc$^+$, $B_{2\alpha}/Y_{5\alpha'}{}^+$), 370 (Fuc-GlcNAcol$^+$, $Y_{1\alpha}{}^+$), and 512 (Gal-(Fuc–)GlcNAc$^+$, $B_{2\alpha}{}^+$) indicate that Fuc residues link to both the non-reducing end like Lewis a/x, and the inner trimannosyl core GlcNAc. Other ions detected at *m/z* 1553 ($Z_{3\gamma}{}^+$, $[Y_{3\gamma}\text{-}H_2O]^+$) and 1570 ($Y_{3\gamma}{}^+$) suggest a linkage of non-substituted HexNAc at the terminal end. From these characteristic ions together with a Y ion at *m/z* 938.03 ($Y_{3\alpha/3\beta}{}^+$), it can be deduced that this HexNAc is a bisecting GlcNAc that attaches to the core mannose residue via β1–4 linkage. On the basis of these product ions, the oligosaccharide is assigned to the structure indicated in Fig. 6A, inset.

3.2.2.2. Fuc-Gal-(Fuc–)GlcNAc–(Lewis b/y type). Fig. 6B is the product ion spectrum of a difucosylated oligosaccharide, $dHex_2Hex_5HexNAc_4HexNAcol_1$, at *m/z* 1070 (9.2 min). The characteristic ions at *m/z* 512 (Gal-(Fuc–)GlcNAc$^+$, Fuc-Gal-GlcNAc$^+$, $B_{3\alpha'}/Y_{6\alpha'''}{}^+$, $B_{3\alpha'}/Y_{5\alpha''''}{}^+$) and 1915 ($B_6{}^+$) suggest the absence of Fuc at the reducing end GlcNAc; a B ion at *m/z* 658 ($B_{3\alpha'}{}^+$), a B/Y ion at *m/z* 350, and a Y ion at *m/z* 1408 ($Y_{3\beta/4\alpha''}{}^+$) suggest the attachment of two Fuc to Gal-GlcNAc at the non-reducing end, in a similar manner to the Lewis b/y antigen, Fuc-Gal-(Fuc–)GlcNAc–. A Y ion at *m/z* 1936 ($Y_{4\alpha''}{}^+$) indicates a linkage of non-substituted HexNAc at the terminal end. A B/Y ion at *m/z* 877 ($B_{4\alpha}/Y_{5\alpha''''}{}^+$, $B_{4\alpha}/Y_{6\alpha'''}{}^+$) and a Y ion at *m/z* 1610 ($Y_{3\beta}{}^+$) suggest that this non-substituted HexNAc residue is linked to the mannose residue attached to the Fuc-Gal-(Fuc–)GlcNAc– structure. These ions lead to assignment of this oligosaccharide as the structure indicated in Fig. 6B, inset.

3.2.2.3. NeuAc-Gal-(NeuAc–)GlcNAc–. Fig. 7A shows the product ion spectrum of a disialylated oligosaccharide, $NeuAc_2dHex_1Hex_5HexNAc_2HexNAcol_1$, at *m/z* 1085 (30.4 min). Characteristic fragment ions at *m/z* 495 ($B_{3\alpha}/Y_{5\alpha'}{}^+$), 948 ($B_{3\alpha}{}^+$), and 1110 ($B_{4\alpha}{}^+$), together with B ions at *m/z* 453 ($B_{2\alpha'}{}^+$) and 657 ($B_{3\alpha}/Y_{5\alpha''}{}^+$, $B_{3\alpha}/Y_{6\alpha'}{}^+$) suggest the presence of a partial structure of NeuAc-Gal-(NeuAc–)GlcNAc–. Furthermore, detection of Y ions at *m/z* 370 ($Y_{1\alpha}{}^+$) and 1059 ($Y_{3\alpha}{}^+$, $Y_{4\alpha/4\beta}{}^+$) as well as a B ion at *m/z* 1799 ($B_6{}^+$) indicate the linkage of a Fuc residue at the inner trimannosyl core GlcNAc. Based on these product ions, the oligosaccharide detected at *m/z* 1085 was assigned to the structure in Fig. 7A, inset.

Table 1
Summary of N-linked oligosaccharides of rat brain Thy-1

Monosaccharidic composition[a]				Theoretical mass[b]	Positive ion mode		Negative ion mmode		Deduced structure[d]
dHex	Hex	HX	NA		Observed *m/z*[c]	Retention time (min)	Observed *m/z*[c]	Retention time (min)	
1	3	2	0	1058.40	1059.46(1)	29.17			CoreF
0	5	2	0	1236.45	1237.47(1)	24.74	1235.45(1)	24.76	M5
0	3	4	0	1318.50	1319.57(1)	8.63			
0	6	2	0	1398.50	1399.53(1)	18.73	1397.50(1)	18.68	M6
0	5	3	0	1439.53	1440.59(1)	9.17			
1	3	4	0	1464.56	733.31(2), 1465.65(1)	23.44			
0	3	5	0	1521.58	761.80(2)	8.63			BisectGN
0	7	2	0	1560.55	781.29(2), 1561.60(1)	18.66			M7
1	5	3	0	1585.59	793.82(2)	14.59			Hybrid
1	5	3	0	1585.59	793.81(2)	19.13			
1	5	3	0	1585.59	793.83(2)	20.96			
0	5	4	0	1642.61	822.33(2)	9.48			Hybrid
0	5	4	0	1642.61	822.33(2)	14.02			
1	3	5	0	1667.64	834.83(2), 1668.69(1)	16.48	832.81(2)	16.44	CoreF
0	4	5	0	1683.63	842.85(2)	17.48			Hybrid
0	8	2	0	1722.61	870.83(2)[e]	17.07			M8
0	5	3	1	1730.62	866.34(2)	20.31			
0	5	3	1	1730.62	866.35(2)	28.91	864.31(2), 1729.64(1)	28.93	Hybrid
2	5	3	0	1731.64	866.86(2)	20.83	864.81(2)	20.85	Hybrid, CoreF, Lax
1	6	3	0	1747.64	874.84(2)	19.19			
2	4	4	0	1772.67	887.37(2)	23.84	885.33(2)	23.86	
2	4	4	0	1772.67	887.36(2)	24.25	885.33(2)	24.27	Hybrid, CoreF, BisectGN
1	5	4	0	1788.67	895.36(2)	7.37			Hybrid
1	5	4	0	1788.67	895.36(2)	13.90			
1	5	4	0	1788.67	895.35(2)	14.16			Hybrid, CoreF
1	5	4	0	1788.67	895.35(2)	19.44	893.33(2)	19.46	Hybrid, CoreF
0	6	4	0	1804.66	903.35(2)	17.07	901.33(2)	17.09	Hybrid, BisectGN
1	4	5	0	1829.69	915.88(2)	8.63			Hybrid
1	4	5	0	1829.69	915.88(2)	9.17			Hybrid
1	4	5	0	1829.69	915.89(2)	18.00			Hybrid
1	4	5	0	1829.69	915.89(2)	22.61	913.84(2)	22.63	
1	5	3	1	1876.68	939.37(2)	21.17	937.34(2)	21.12	
1	5	3	1	1876.68	939.36(2)	24.90	937.34(2)	24.92	
1	5	3	1	1876.68	939.39(2)	32.76	937.33(2)	32.78	Hybrid, CoreF
0	9	2	0	1884.66	951.88(2)[e]	17.53			M9
0	6	3	1	1892.68	947.39(2)	23.31	945.33(2)	23.33	Hybrid
0	6	3	1	1892.68	947.39(2)	31.09	945.33(2)	31.05	Hybrid
2	6	3	0	1893.70	947.87(2)	24.61	945.84(2)	24.70	
1	4	4	1	1917.71			957.85(2)	27.73	
1	4	4	1	1917.71			957.85(2)	28.86	
1	4	4	1	1917.71			957.85(2)	34.91	CoreF
1	4	4	1	1917.71			957.85(2)	35.55	
0	5	4	1	1933.70	967.89(2)	22.61	965.85(2)	22.63	Hybrid
0	5	4	1	1933.70	967.86(2)	24.61	965.82(2)	24.70	
2	5	4	0	1934.72	968.39(2)	13.97			Hybrid
1	6	4	0	1950.72	976.39(2)	9.93			Hybrid, Lax
1	6	4	0	1950.72	976.41(2)	21.76	974.35(2)	21.79	Hybrid, CoreF
2	4	5	0	1975.75	988.90(2)	16.21	986.85(2)	16.16	Complex
2	4	5	0	1975.75	988.90(2)	17.07	986.87(2)	17.09	Complex
0	5	3	2	2021.72			1009.86(2)	26.35	
0	5	3	2	2021.72			1009.85(2)	26.83	
1	6	3	1	2038.73	1020.40(2)	23.84	1018.36(2)	23.80	
1	6	3	1	2038.73	1020.44(2)	27.77	1018.37(2)	27.80	CoreF
1	6	3	1	2038.73	1020.42(2)	34.66	1018.36(2)	34.69	Hybrid, CoreF
1	5	4	1	2079.76	1040.92(2)	25.73	1038.87(2)	25.81	CoreF
1	5	4	1	2079.76	1040.92(2)	29.04	1038.88(2)	28.99	
3	5	4	0	2080.78	1041.42(2)	23.84	1039.39(2)	23.86	
0	6	4	1	2095.76	1048.94(2)	20.57			Hybrid
0	6	4	1	2095.76	1048.91(2)	23.84	1046.87(2)	23.80	Hybrid
2	6	4	0	2096.78	1049.42(2)	7.58			

Table 1 (*Continued*)

Monosaccharide composition[a]				Theoretical mass[b]	Positive ion mode		Negative ion mnmode		Deduced structure[d]
dHex	Hex	HX	NA		Observed *m/z*[c]	Retention time (min)	Observed *m/z*[c]	Retention time (min)	
2	6	4	0	2096.78	1049.42(2)	15.97			
2	6	4	0	2096.78	1049.42(2)	16.61			Hybrid, BisectGN
2	6	4	0	2096.78	1049.43(2)	25.73			
1	7	4	0	2112.77			1055.38(2)	34.62	
1	4	5	1	2120.79	1061.45(2)	20.43			Complex
1	4	5	1	2120.79	1061.45(2)	24.74	1059.39(2)	24.70	
1	4	5	1	2120.79	1061.45(2)	26.47	1059.39(2)	26.42	CoreF
2	5	5	0	2137.80	1069.94(2)	9.17			Lby
2	5	5	0	2137.80	1069.94(2)	21.30			
2	5	5	0	2137.80	1069.95(2)	23.09	1067.9(2)	23.04	
1	5	3	2	2167.78	1084.94(2)	30.41	1082.89(2)	30.37	Hybrid, CoreF
2	4	6	0	2178.83	1090.45(2)	26.08			
0	6	3	2	2183.77	1092.95(2)	28.63	1090.88(2)	28.60	Hybrid, diSia
0	5	4	2	2224.80	1113.45(2)	26.10			
2	5	4	1	2225.82	1113.95(2)	27.56			
2	5	4	1	2225.82	1113.98(2)	34.80			
1	6	4	1	2241.81	1121.95(2)	26.60	1119.90(2)	26.63	
1	6	4	1	2241.81			1119.90(2)	30.58	
1	6	4	1	2241.81			1119.91(2)	38.14	
3	6	4	0	2242.83	1122.46(2)	14.23			
2	7	4	0	2258.83	1130.46(2)	10.47			
3	5	5	0	2283.86	1142.96(2)	16.87			
1	4	6	1	2323.87	1162.98(2)	26.60			
1	6	3	2	2329.83			1163.91(2)	31.72	
1	6	3	2	2329.83			1163.91(2)	32.54	Hybrid, diSia
1	5	4	2	2370.86	1186.55(2)	29.89	1184.42(2)	30.00	Complex, CoreF
1	5	4	2	2370.86			1184.43(2)	36.00	
1	5	4	2	2370.86	1186.52(2)	36.31	1184.42(2)	36.40	Complex, CoreF
1	5	4	2	2370.86	1186.50(2)	42.47	1184.43(2)	42.43	Complex, CoreF
3	5	4	1	2370.86			1184.93(2)	30.99	
2	5	5	1	2428.90	1215.50(2)	21.17	1213.44(2)	21.25	
2	5	5	1	2428.90	1215.50(2)	23.84			
2	5	5	1	2428.90	1215.52(2)	26.32	1213.45(2)	26.28	
2	5	5	1	2428.90	1215.50(2)	27.50	1213.45(2)	27.53	
2	5	4	2	2516.91	1259.60(2)	32.23	1257.45(2)	32.19	Complex, Lax, CoreF, diSia
2	5	4	2	2516.91			1257.45(2)	36.72	
2	5	6	1	2631.98			876.32(3), 1314.99(2)	26.76	
3	5	4	2	2662.97			1330.49(2)	32.78	
1	5	6	2	2777.02			1387.50(2)	30.99	
0	6	5	3	2881.03			1439.50(2)	34.83	
0	6	5	3	2881.03			1439.49(2)	40.77	
2	6	5	2	2882.05			1440.05(2)	37.96	
2	6	6	2	3085.13			1541.55(2)	31.38	

[a] dHex, deoxyhexose; Hex, hexose; HX, *N*-acetylhexamine; NeuAc, *N*-acetylneuramic acid.
[b] Monoisotopic value.
[c] Values in parentheses are charge state.
[d] Structures are deduced by MS^n. Complex, complex-type-oligosaccharide; Hybrid, hybrid-type-oligosaccharide; M5-9, high-mannose-type oligosaccharide containing 5–9 mannose residues; BisectGN, bisecting GlcNAc; Lax, Lewis a/x structure; Lby, Lewis b/y structure; diSia, disialic acid.
[e] Ammonium adducted form.

3.2.2.4. NeuAc-Gal-GlcNAc–. Fig. 7B shows the product ion spectrum of a disialylated oligosaccharide, $NeuAc_2dHex_1Hex_5HexNAc_3HexNAcol_1$, at *m/z* 1187 (42.5 min). Although B ions were detected at *m/z* 454 (B_{2x}^+), 657 (B_{3x}^+) and 819 (B_{4x}^+), none of the fragment ions at *m/z* 495 (NeuAc-GlcNAc$^+$), 948 (NeuAc-Gal-(NeuAc–)GlcNAc$^+$), or 1110 (NeuAc-Gal-(NeuAc–)GlcNAc-Man$^+$) were detected in the spectrum. This result suggests that the two NeuAc residues occupy both non-reducing ends of the biantennary form. Fucosylation of the inner trimannnosyl core GlcNAc was determined by the detection of Y ions at *m/z* 370 ($Y_{1\alpha}^+$) and 1059 ($Y_{4\alpha/4\beta}^+$). These product ions lead to assignment of this oligosaccharide the structure in Fig. 6B.

3.2.2.5. (v) NeuAc-NeuAc–. Fig. 7C shows the product ion spectrum of a disialylated and difucosylated oligosaccharide, $NeuAc_2dHex_2Hex_5HexNAc_3HexNAcol_1$, at *m/z* 1260 (32.2 min). The characteristic ions at *m/z* 583 (NeuAc-NeuAc$^+$,

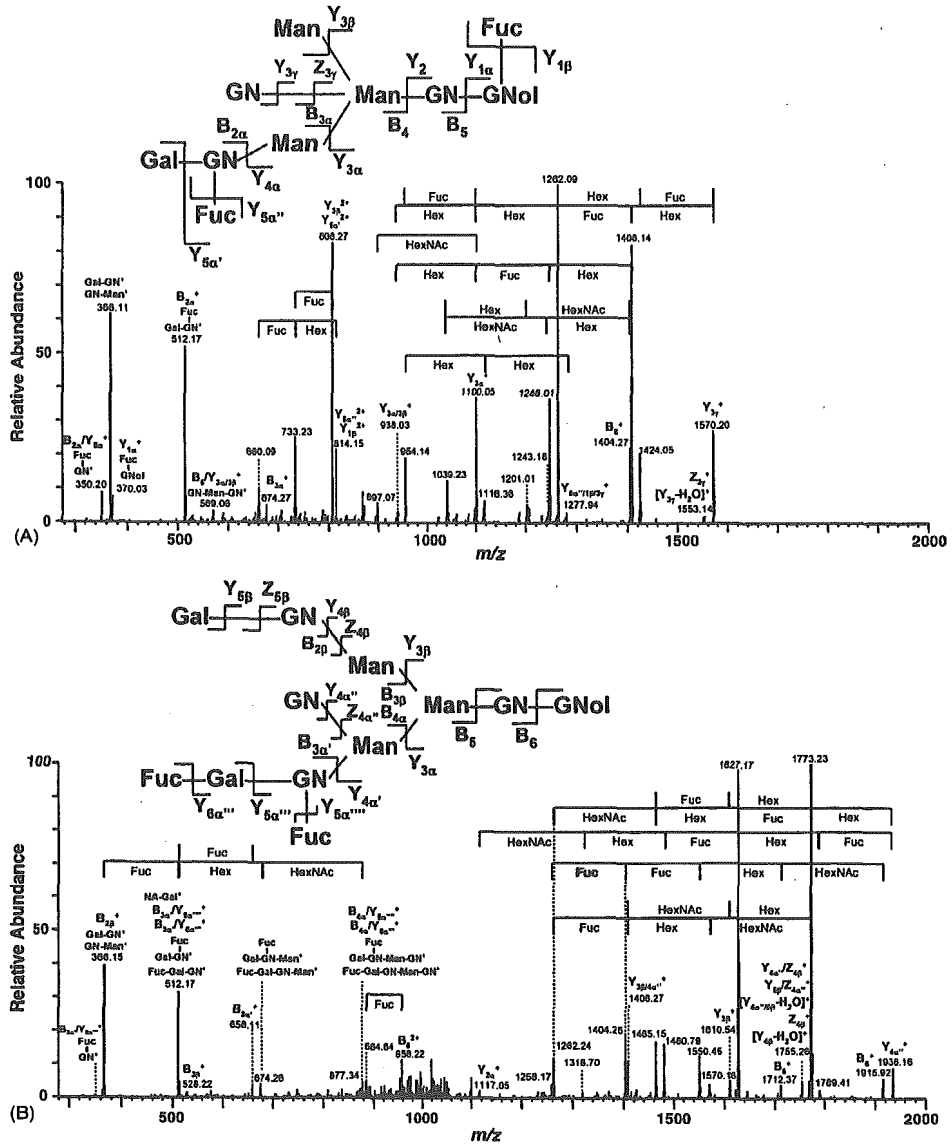

Fig. 6. Product ion spectra of N-linked oligosaccharides of rat brain Thy-1. (A) MS^2 spectrum of $dHex_2Hex_4HexNAc_3HexNAcol_1$ at *m/z* 887 (24.3 min). (B) MS^2 spectrum of $dHex_2Hex_5HexNAc_4HexNAcol_1$ at *m/z* 1070 (9.2 min).

$B_{2\alpha'}{}^+$), 949 (NeuAc-NeuAc-Gal-GlcNAc$^+$, $B_{3\alpha}/Y_{5\alpha''}{}^+$), and 1094 (NeuAc-NeuAc-Gal-(Fuc−)GlcNAc$^+$, $B_{3\alpha}{}^+$) suggest that this oligosaccharide contains a disialic acid residue and one Fuc at the non-reducing end. In addition, a Y ion at *m/z* 370 ($Y_{1\alpha}{}^+$) indicated that the other Fuc was attached to GlcNAc at the reducing end. Based on these product ions, this oligosaccharide structure could be assigned as indicated in Fig. 7C, inset.

4. Discussion

Thy-1 has three *N*-glycosylation sites, Asn23, 74, and 98. We have previously demonstrated the attachment of high-mannose-type, complex-type, and hybrid-type oligosaccharides to these sites. Asn74 is occupied with various *N*-glycans, which have been estimated to be fucosylated and sialylated [31]. Product ion spectra containing fucosylation and sialylation isomers make it difficult to elucidate the detailed structure. We have conducted mass spectrometric oligosaccharide analysis through the separation of diverse oligosaccharides with GCC. We first improved the mass spectrometric oligosaccharide profiling by IT–MS-FT–ICR–MS. The improved method enabled the monosaccharide composition analysis and sequencing of both neutral and acidic oligosaccharides in a single run. Using this method, we successfully analyzed various *N*-glycans of Thy-1 that could not be characterized by the analysis of glycopeptides. We found a Lewis b/y structure and sialylated GlcNAc in the branch structure. Interestingly, disialic acid (NeuAc-NeuAc−), which is known to be involved in neurite formation was found in brain Thy-1 [38].

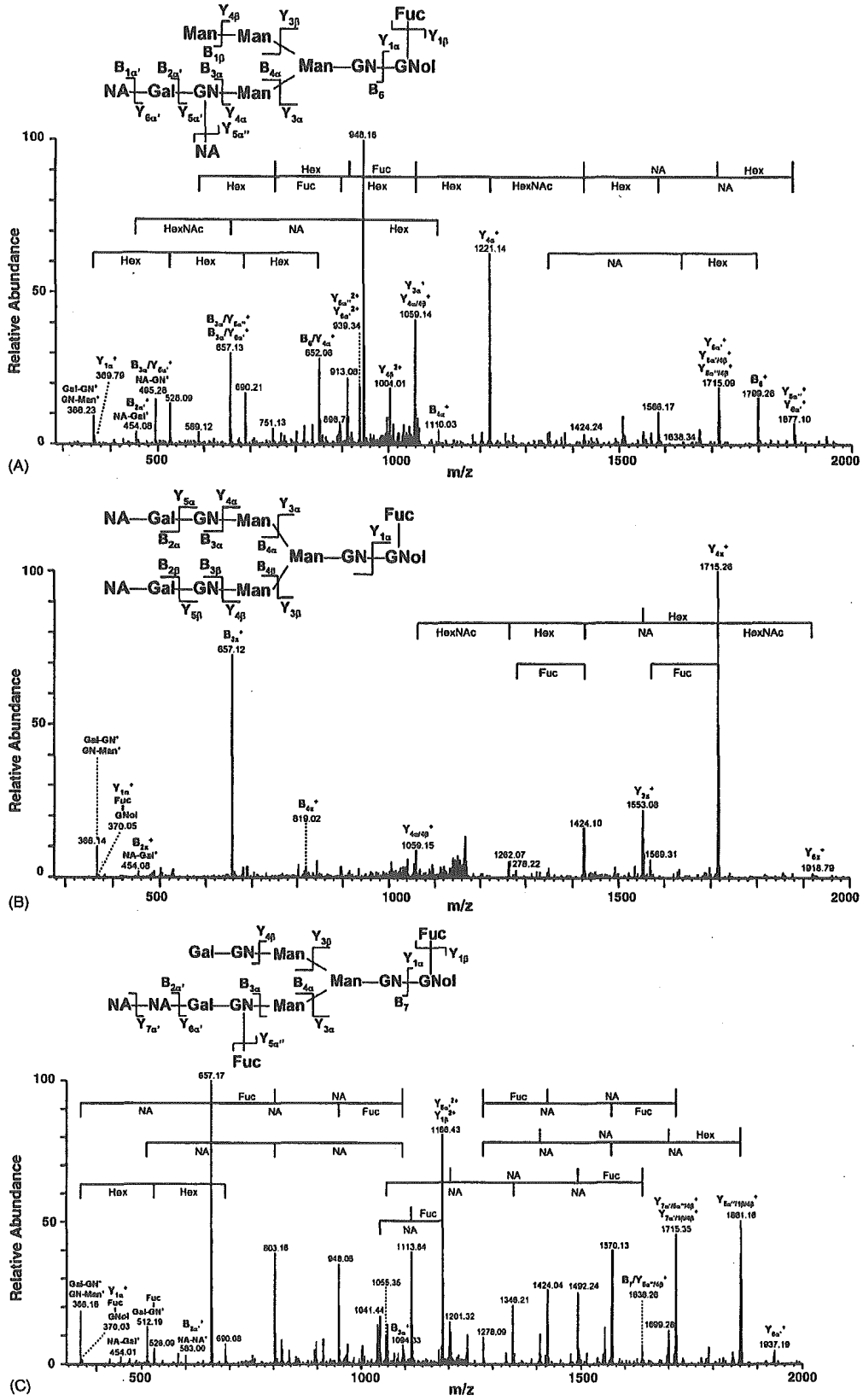

Fig. 7. Production spectra of N-linked oligosaccharides of rat brain Thy-1. (A) MS^2 spectrum of $NeuAc_2dHex_1Hex_5HexNAc_2HexNAcol_1$ at *m/z* 1085 (30.4 min). (B) MS^2 spectrum of $NeuAc_2dHex_1Hex_5HexNAc_3HexNAcol_1$ at *m/z* 1187 (42.5 min). (C) MS^2 spectrum of $NeuAc_2dHex_2Hex_5HexNAc_3HexNAcol_1$ at *m/z* 1260 (32.2 min).

In these two studies, we have demonstrated a strategy for glycosylation analysis of Thy-1, including identification of a glycoprotein, determination of glycosylation sites, site-specific glycosylation analysis, and structural analysis of oligosaccharide details. This strategy can be applied to glycosylation analysis of other glycoproteins. Specifically, the glycoprotein sample is divided into two. One is subjected to proteinase digestion followed by peptide/glycopeptide mapping, which provides information on glycosylation sites and site-specific heterogeneity. The other is subjected to PNGase F digestion followed by mass spectrometric oligosaccharide profiling, by which a detailed structure of *N*-glycans released from a glycoprotein could be provided. Recently, proteomic approaches, which are based on two-dimensional electrophoresis followed by mass spectrometry, have been used in various fields. Although glycosylation analysis of abundant glycoproteins in gel has been successful, that of a low-abundance glycoprotein in gel remains a great challenge. The proposed method consisting of peptide/glycopeptide mapping followed by oligosaccharide profiling with sequential scans by IT–MS-FT–ICR–MS will likely be a powerful tool for glycosylation analysis of low-abundance glycoproteins and for proteomics/glycomics.

Acknowledgements

This work was supported in part by a Grant-in-Aid for Creative Scientific Research (16GS0313) from the Ministry of Education, Culture, Sports, and Technology, the Ministry of Health, Labor and Welfare, and Core Research for the Evolutional Science and Technology Program (CREST) of the Japan Science and Technology Agency (JST).

We appreciate Dr. A. Hachisuka of the National Institute of Health Science for her technical advice.

We thank Dr. M. Kubota and Mr. M. Yoshida of Thermo Electron K.K. (Japan) for their technical support.

References

[1] A. Varki, Glycobiology 3 (1993) 97.
[2] J.W. Dennis, M. Granovsky, C.E. Warren, Biochim. Biophys. Acta 1473 (1999) 21.
[3] Y. Sato, M. Kimura, C. Yasuda, Y. Nakano, M. Tomita, A. Kobata, T. Endo, Glycobiology 9 (1999) 655.
[4] G. Durand, N. Seta, Clin. Chem. 46 (2000) 795.
[5] O. Krokhin, W. Ens, K.G. Standing, J. Wilkins, H. Perreault, Rapid Commun. Mass Spectrom. 18 (2004) 2020.
[6] Y. Satomi, Y. Shimonishi, T. Takao, FEBS Lett. 576 (2004) 51.
[7] Y. Wada, M. Tajiri, S. Yoshida, Anal. Chem. 76 (2004) 6560.
[8] W. Chai, V. Piskarev, A.M. Lawson, Anal. Chem. 73 (2001) 651.
[9] D. Sagi, J. Peter-Katalinic, H.S. Conradt, M. Nimtz, J. Am. Soc. Mass Spectrom. 13 (2002) 1138.
[10] A. Zamfir, D.G. Seidler, H. Kresse, J. Peter-Katalinic, Glycobiology 13 (2003) 733.
[11] D.J. Harvey, R.L. Martin, K.A. Jackson, C.W. Sutton, Rapid Commun. Mass Spectrom. 18 (2004) 2997.
[12] C. Robbe, C. Capon, B. Coddeville, J.C. Michalski, Rapid Commun. Mass Spectrom. 18 (2004) 412.
[13] N. Ojima, K. Masuda, K. Tanaka, O. Nishimura, J. Mass Spectrom. 40 (2005) 380.
[14] C.W. Sutton, J.A. O'Neill, J.S. Cottrell, Anal. Biochem. 218 (1994) 34.
[15] B. Küster, S.F. Wheeler, A.P. Hunter, R.A. Dwek, D.J. Harvey, Anal. Biochem. 250 (1997) 82.
[16] B. Küster, T.N. Krogh, E. Mortz, D.J. Harvey, Proteomics 1 (2001) 350.
[17] K. Hirayama, R. Yuji, N. Yamada, K. Kato, Y. Arata, I. Shimada, Anal. Chem. 70 (1998) 2718.
[18] F. Wang, A. Nakouzi, R.H. Angeletti, A. Casadevall, Anal. Biochem. 314 (2003) 266.
[19] K. Sandra, I. Stals, P. Sandra, M. Claeyssens, J. Van Beeumen, B. Devreese, J. Chromatogr. A 1058 (2004) 263.
[20] Y. Satomi, Y. Shimonishi, T. Hase, T. Takao, Rapid Commun. Mass Spectrom. 18 (2004) 2983.
[21] A. Harazono, N. Kawasaki, T. Kawanishi, T. Hayakawa, Glycobiology 15 (2005) 447.
[22] M. Wuhrer, C.A. Koeleman, C.H. Hokke, A.M. Deelder, Anal. Chem. 77 (2005) 886.
[23] B.L. Schulz, N.H. Packer, N.G. Karlsson, Anal. Chem. 74 (2002) 6088.
[24] N.L. Wilson, B.L. Schulz, N.G. Karlsson, N.H. Packer, J. Proteome Res. 1 (2002) 521.
[25] L.A. Gennaro, D.J. Harvey, P. Vouros, Rapid Commun. Mass Spectrom. 17 (2003) 1528.
[26] N.G. Karlsson, B.L. Schulz, N.H. Packer, J. Am. Soc. Mass Spectrom. 15 (2004) 659.
[27] N.G. Karlsson, N.L. Wilson, H.J. Wirth, P. Dawes, H. Joshi, N.H. Packer, Rapid Commun. Mass Spectrom. 18 (2004) 2282.
[28] M. Wuhrer, C.A. Koeleman, A.M. Deelder, C.H. Hokke, Anal. Chem. 76 (2004) 833.
[29] Y. Takegawa, K. Deguchi, S. Ito, S. Yoshioka, H. Nakagawa, S. Nishimura, Anal. Chem. 77 (2005) 2097.
[30] S. Itoh, N. Kawasaki, M. Ohta, T. Hayakawa, J. Chromatogr. A 978 (2002) 141.
[31] S. Itoh, N. Kawasaki, A. Harazono, N. Hashii, Y. Matsuishi, T. Kawanishi, T. Hayakawa, J. Chromatogr. A 1094 (2005) 105.
[32] N. Kawasaki, M. Ohta, S. Hyuga, O. Hashimoto, T. Hayakawa, Anal. Biochem. 269 (1999) 297.
[33] S. Itoh, N. Kawasaki, M. Ohta, M. Hyuga, S. Hyuga, T. Hayakawa, J. Chromatogr. A 968 (2002) 89.
[34] N. Kawasaki, S. Itoh, M. Ohta, T. Hayakawa, Anal. Biochem. 316 (2003) 15.
[35] C. Bordier, J. Biol. Chem. 256 (1981) 1604.
[36] M.P. Lisanti, M. Sargiacomo, L. Graeve, A.R. Saltiel, E. Rodriguez-Boulan, Proc. Natl. Acad. Sci. U.S.A. 85 (1988) 9557.
[37] B. Domon, C.E. Costello, Glycoconjugate J. 5 (1988) 397.
[38] C. Sato, T. Matsuda, K. Kitajima, J. Biol. Chem. 277 (2002) 45299.

RAPID COMMUNICATIONS IN MASS SPECTROMETRY
Rapid Commun. Mass Spectrom. 2005; 19: 3315–3321
Published online 31 October 2005 in Wiley InterScience (www.interscience.wiley.com). DOI: 10.1002/rcm.2190

Specific detection of Lewis x-carbohydrates in biological samples using liquid chromatography/multiple-stage tandem mass spectrometry

Noritaka Hashii[1,2], Nana Kawasaki[1,2]*, Satsuki Itoh[1], Akira Harazono[1], Yukari Matsuishi[1,2], Takao Hayakawa[3] and Toru Kawanishi[1]

[1]Division of Biological Chemistry and Biologicals, National Institute of Health Sciences, 1-18-1 Kamiyoga, Setagaya-ku, Tokyo 158-8501, Japan
[2]Core Research for Evolutional Science and Technology (CREST) of Japan Science and Technology Agency (JST), Kawaguchi Center Building, 4-1-8 Hon-cho, Kawaguchi, Saitama 332-0012, Japan
[3]Pharmaceutical and Medical Devices Agency, 3-3-2 Kasumigaseki, Chiyoda-ku, Tokyo 100-0013, Japan

Received 14 July 2005; Revised 5 September 2005; Accepted 8 September 2005

The Lewis x structure [Le^x, Galβ1-4(Fucα1-3)GlcNAc] motif is one of the tumor antigens and plays an important role in oncogenesis, development, cellular differentiation and adhesion. The detection of Le^x-carbohydrates and their structural analysis are necessary to clarify the role of Le^x in several biological events. Mass spectrometry has been preferably used for the structural analysis of carbohydrates. Especially, collision-induced dissociation (CID) tandem mass spectrometry (MS/MS), which causes a glycosidic bond cleavage, is used for carbohydrate sequencing. However, Le^x cannot be identified by MS/MS due to the existence of the positional isomers, such as Lewis a [Galβ1-3(α1-4Fuc)GlcNAc]. In the present study, we demonstrate the specific detection of Le^x-carbohydrates in a biological sample by using multiple-stage MS/MS (MS^n). Using pyridylaminated oligosaccharides bearing Le^x, we found that the Le^x-motif yields a cross-ring fragment by the cleavage of a bond between C-3 and C-4 of GlcNAc in Gal(Fuc)GlcNAc. The Le^x-specific cross-ring fragment ion at *m/z* 259 was effectively detected by sequential scans, consisting of a full MS^1 scan, data-dependent CID MS^2 scan, MS^3 of $[Gal(Fuc)GlcNAc+Na]^+$ at *m/z* 534, and MS^4 of $[GalGlcNAc+Na]^+$ at *m/z* 388. The sequential scan was applied to *N*-linked oligosaccharide profiling using a LC/ESI-MS^n system equipped with a graphitized carbon column. We successfully detected the Le^x-motif and elucidated the structures of several Le^x and Lewis y [(Fucα1-2)Galβ1-4(Fucα1-3)GlcNAc] oligosaccharides in the murine kidney used as a model tissue. Our method is expected to be a powerful tool for the specific detection of the Le^x-motif, and structural elucidation of Le^x-carbohydrates in biological samples. Copyright © 2005 John Wiley & Sons, Ltd.

The Lewis x structure [Le^x, Galβ1-4(Fucα1-3)GlcNAc] is one of the tumor antigens, and plays an important role in oncogenesis[1,2] (abbreviations used here are: Gal, galactose; Fuc, fucose; GlcNAc, *N*-acetylglucosamine). Particularly, sialylated Le^x is used as a marker of lung, pancreas and uterus tumors.[3] Le^x and its derivatives are also known to be oligosaccharide ligands of some endothelial receptors, such as the selectins and the scavenger receptor, C-type lectin,[4,5] and affect embryonic development, cellular differentiation and adhesion.[6,7] However, the structural details of the oligosaccharides attached to the Le^x structure (Le^x-oligosaccharide) are still unclear. Le^x structure-specific detection and elucidation methods are necessary for the diagnosis of tumors and a study on the role of Le^x on various biological events.

Mass spectrometry (MS) has become very popular for the structural analysis of oligosaccharides. Low-energy collision-induced dissociation (CID) tandem mass spectrometry (MS/MS), which generates B/Y-series ions by glycosidic bond cleavage, is preferably used for oligosaccharide sequencing.[8–13] However, the detection of Le^x by MS/MS is still challenging due to the presence of its positional isomer, Lewis a [Le^a, Galβ1-3(Fucα1-4)GlcNAc]. The structural difference between Le^x and Le^a is the linkage at positions 3 or 4 of the non-reducing terminal fucose and galactose to GlcNAc (Fig. 1). For the linkage analysis, multiple-stage MS/MS (MS^n) pattern-matching, in which the oligosaccharide structure can be deduced from intensity ratios of fragment ions generated by MS^n, has recently been reported;[14–16] however, this method needs an identical analytical condition and various oligosaccharide standards. As an alternative method, the cross-ring fragmentation caused by MS^n is

*Correspondence to: N. Kawasaki, Division of Biological Chemistry and Biologicals, National Institute of Health Sciences, 1-18-1 Kamiyoga, Setagaya-ku, Tokyo 158-8501, Japan.
E-mail: nana@nihs.go.jp
Contract/grant sponsor: Ministry of Health Labor and Welfare, and Core Research for the Evolutional Science and Technology Program, Japan Science and Technology Corp.

RCM

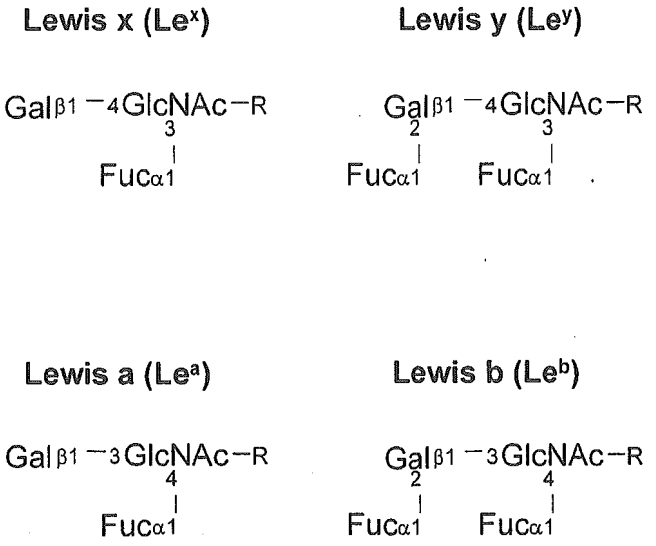

Figure 1. Structures of Lewis a, b, x and y.

sometimes used.[10,17,18] Meisen *et al.*[19] demonstrated that α2-6-linked *N*-acetylneuraminic acid (NeuNAc) can be distinguished from α2-3-linked NeuNAc based on structure-specific cross-ring fragment ions generated by low-energy CID MS^2 in the negative ion mode. Le^x could be expected to be distinguished from its positional isomers by cross-ring fragmentation.

In this study, we demonstrate the specific detection of Le^x-carbohydrates in a biological sample by using MS^n. Using pyridylaminated oligosaccharides bearing Le^x, we found that the Le^x-motif yields a cross-ring fragment by the cleavage of a bond between C-3 and C-4 of GlcNAc in Gal(Fuc)GlcNAc. The Le^x-specific cross-ring fragment ion at *m/z* 259 was effectively detected by sequential scans, consisting of a full MS^1 scan, data-dependent CID MS^2 scan, MS^3 of $[Gal(Fuc)GlcNAc+Na]^+$ at *m/z* 534, and MS^4 of $[GalGlcNAc+Na]^+$ at *m/z* 388 using nano-electrospray ionization-ion trap mass spectrometry (nanoESI-ITMS) in positive ion mode. Then, sequential MS^{1-4} scanning for the Le^x-characteristic ions was applied for *N*-linked oligosaccharide profiling using an LC/ESI-ITMS instrument equipped with a graphitized carbon column (GCC), by which diverse oligosaccharides, including isomers, can be separated. We successfully detected the Le^x-motif and subsequently elucidated the entire structure of Le^x-oligosaccharides in the model tissue, murine kidney, in which Le^x-oligosaccharides are abundantly present.[20]

EXPERIMENTAL

Materials

2-Aminopyridine (PA)-labeled pentasaccharides bearing Le^x (oligosaccharide I, Fig. 2(A)) or Le^a (oligosaccharide II, Fig. 2(B)), and the asialotriantennary oligosaccharide bearing Le^x (oligosaccharide III, Fig. 2(C)), were purchased from Takara Biomedicals (Otsu, Japan). Murine kidneys (MRL/MpJ-+/+) were purchased from Japan SLC Inc. (Hamamatsu, Japan).

Sample preparation

Proteins from murine kidneys were solubilized in lysis buffer (7 M urea, 2 M thiourea, 2% CHAPS, 30 mM Tris-HCl) by vortexing at room temperature. The proteins (100 μg) were recovered by precipitation in cold acetone, and then treated with 10 units of PNGase F in 500 μL of 0.2 M phosphate buffer (pH 7.6) at 37°C for 48 h to release the *N*-linked oligosaccharides. Proteins were removed by precipitation in cold ethanol, and the supernatant containing oligosaccharides was evaporated and lyophilized. The dried oligosaccharides were labeled with PA according to a previous report.[21] The PA-labeled oligosaccharides were desalted with Envi-Carb C (Supelco Bellefonte, USA) and lyophilized.

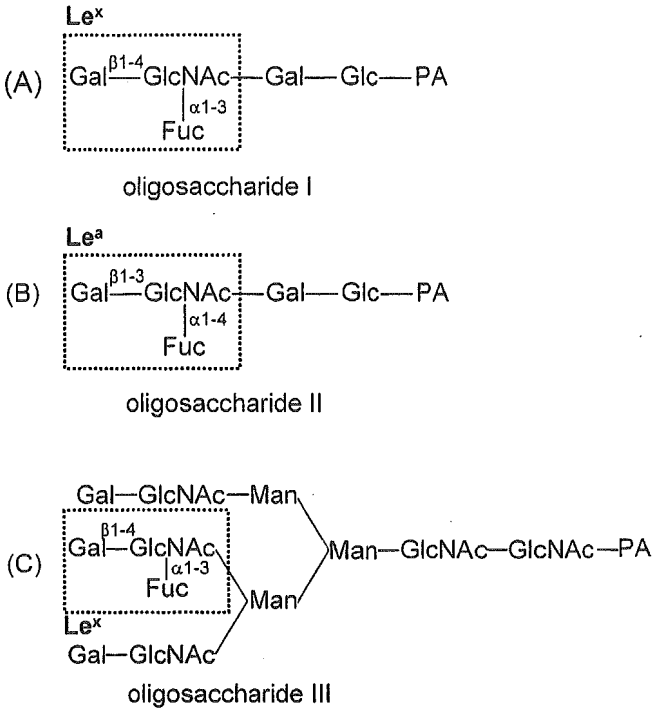

Figure 2. Structures of model oligosaccharides used in this study: (A) PA-labeled Le^x-pentasaccharide (oligosaccharide I); (B) PA-labeled Le^a-pentasaccharide (oligosaccharide II); and (C) PA-labeled Le^x-asialotriantennary complex type oligosaccharide (oligosaccharide III).

nanoESI-MS^n

Experiments were performed using a Finnigan linear ion trap Fourier transform ion cyclotron resonance mass spectrometer (LTQ-FT, ThermoElectron, San Jose, CA, USA) equipped with a nanoESI source (AMR, Inc., Tokyo, Japan). ESI-MS^n was carried out for Le^x- and Le^a-oligosaccharide standards at a concentration of 1 pmol/μL in 5 mM ammonium acetate and 10 μM NaCl buffer (pH 9.6) containing 50% acetonitrile. The sample was analyzed at a flow rate of 2.0 μL/min using a spray voltage of 2.0 kV in the positive ion mode. The capillary temperature was set to 200°C; collision energies were set to 20–30% for the MS^n experiments; the maximum scan time was set to 50 ms. MS^2 and MS^3 were performed with an isolation width of 3.0 u (range of precursor ion ±1.5).

LC/MS^n

LC was carried out using a MAGIC 2002 system (Michrom BioResources, Auburn, CA, USA) equipped with a GCC (Hypercarb column, 150 × 0.2 mm, ThermoElectron). The

eluents were 5 mM ammonium acetate, pH 9.6, containing 2% acetonitrile (pump A) and 5 mM ammonium acetate, pH 9.6, containing 80% acetonitrile (pump B). PA-labeled *N*-linked oligosaccharides from murine kidney were eluted at a flow rate of 2 μL/min with a gradient of 10–70% of pump B in 60 min. A solution of NaCl (10 μM) was passed post-column at a flow rate of 2 μL/min. The precursor ions detected by a full MS^1 scan (mass range at *m/z* 750–2000) were followed by MS^2 scans of the most intense ions.

RESULTS AND DISCUSSION

MS^n of Le^x-pentaoligosaccharide

The model Le^x-pentaoligosaccharide (oligosaccharide I) was analyzed by nanoESI-MS^n with direct injection in the positive ion mode. Sodium chloride (NaCl) was deliberately added to the sample for the acceleration of the cross-ring cleavages according to previous reports.[22–24] The sodiated singly charged molecular ion, $[M+Na]^+$, of oligosaccharide I was observed at *m/z* 954.4 in the MS^1 spectrum (Fig. 3(A)). MS^2 of the sodiated molecular ion yielded $[(M+Na)-Fuc]^+$ at *m/z* 808 as the most intense ion by the glycosidic bond cleavage between GlcNAc and Fuc residues (Fig. 3(B)). This indicates that the Fuc residue is easily dissociated by low-energy CID MS^2. In addition to the defucosylated ions, we observed the sodiated ion at *m/z* 534, corresponding to the Le^x and Le^a structure, $[Gal(Fuc)GlcNAc+Na]^+$. The sodiated B_2 ion (*m/z* 534) was subjected to a further product ion scan, and the sodiated ion at *m/z* 388 corresponding to $[GalGlcNAc+Na]^+$ appeared in the MS^3 spectrum (Fig. 3(C)). The ion at *m/z* 372, corresponding to $[FucGlcNAc+Na]^+$, which proves the attachment of Fuc to GlcNAc, was also detected. Then, MS^4 of the sodiated $Y_{3\alpha}$ ion (*m/z* 388) yielded a sodiated cross-ring fragment ion at *m/z* 259, corresponding to the sodiated $^{3,5}A_2$ ion, which proves the linkage of the Gal residue at position C-4 on GlcNAc, with some neutral losses: 60 Da ($^{0,4}A_2$, $^{0,4}X_{4\beta}$, $^{1,3}X_{4\beta}$ and $^{2,4}X_{4\beta}$) and 90 Da ($^{0,3}X_{4\beta}$ and $^{1,4}X_{4\beta}$) (Fig. 3(D)).

MS^n of Le^a-pentaoligosaccharide

The Le^a-pentasaccharide (oligosaccharide II) was subjected to nanoESI-MS^n in a similar manner. The $[M+Na]^+$ of oligosaccharide II was observed at *m/z* 954.4 in the MS^1 spectrum (Fig. 4(A)). MS^2 of the $[M+Na]^+$ at *m/z* 954 yielded the sodiated ion at *m/z* 534, corresponding to $[Gal(Fuc)GlcNAc+Na]^+$ (Fig. 4(B)). MS^3 of the sodiated B_2 ion (*m/z* 534) yielded the sodiated $Y_{3\alpha}$ and $Y_{3\beta}$ ions at *m/z* 372 and 388, respectively (Fig. 4(C)). MS^4 of the sodiated $Y_{3\beta}$ ion at *m/z* 388 yielded some cross-ring fragment ions at *m/z* 208, 268, 298 and 328, corresponding to neutral losses: 60 Da ($^{0,4}A_2$, $^{0,4}X_{4\beta}$, $^{1,3}X_{4\beta}$ and $^{2,4}X_{4\beta}$) and 90 Da ($^{0,3}A_2$, $^{0,3}X_{4\beta}$ and $^{1,4}X_{4\beta}$) (Fig. 4(D)). $^{3,5}A_2$ at *m/z* 259, which arose from oligosaccharide I, was not detected by MS^4 of Le^a.

These results suggest that the Le^x structure can be identified by the $^{3,5}A_2$ ion at *m/z* 259 generated by MS^4 of $[GalGlcNAc+Na]^+$ at *m/z* 388, which arose from MS^3 $[Gal(Fuc)GlcNAc+Na]^+$ at *m/z* 534 (Fig. 5).

MS^n of Le^x-asialotriantennary oligosaccharide

Using a Le^x-oligosaccharide with a more complicated branching structure, we confirmed the practicability of MS^3 of the ion at *m/z* 534 followed by MS^4 of the ion at *m/z* 388 for the detection of the Le^x-diagnostic ion at *m/z* 259.

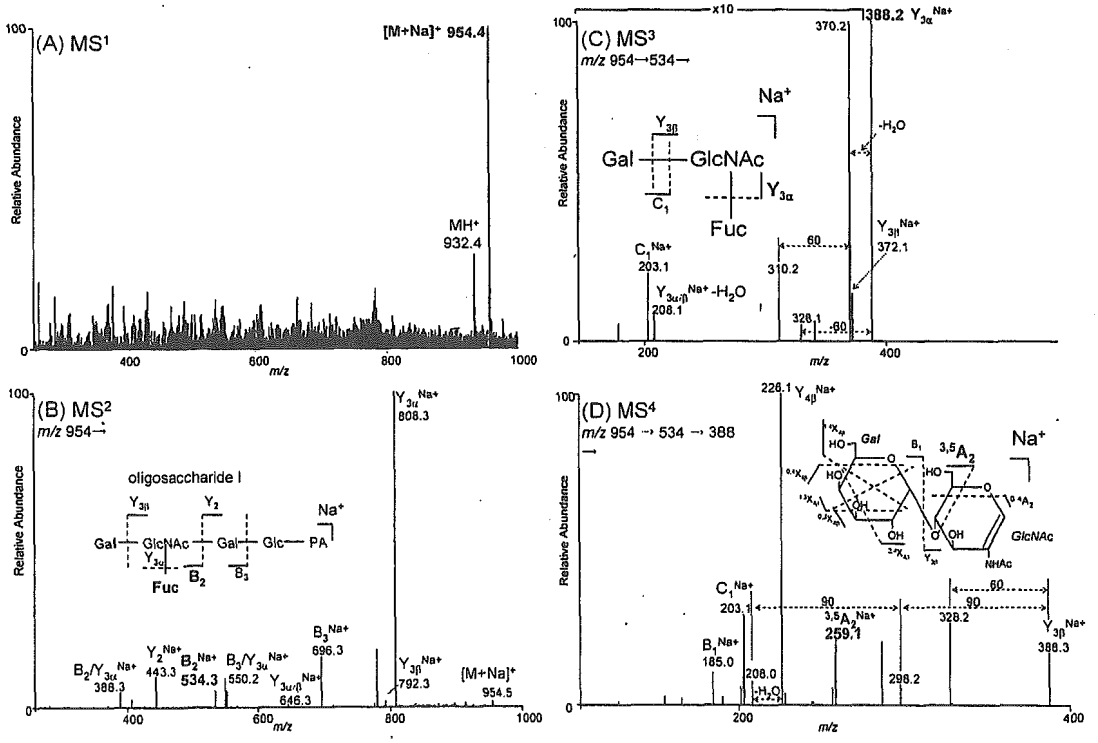

Figure 3. MS$^{1-4}$ spectra of oligosaccharide I by ESI-MS^n: (A) MS^1 spectrum; (B) MS^2 spectrum of $[M+Na]^+$ at *m/z* 954.4; (C) MS^3 spectrum of $[Gal(Fuc)GlcNAc+Na]^+$ at *m/z* 534.3 detected in MS^2; and (D) MS^4 spectrum of $[GalGlcNAc+Na]^+$ at *m/z* 388.2 detected in MS^3.

RCM

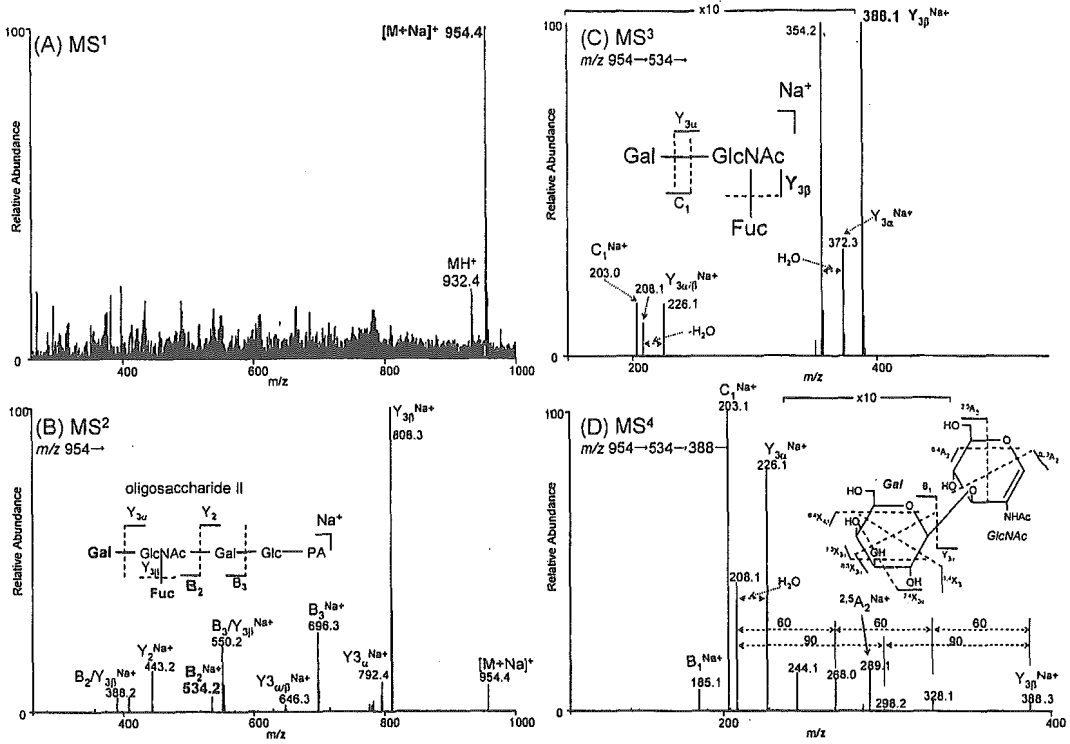

Figure 4. MS^{1-4} spectra of oligosaccharide II by ESI-MS^n: (A) MS^1 spectrum; (B) MS^2 spectrum of $[M+Na]^+$ at *m/z* 954.4; (C) MS^3 spectrum of $[Gal(Fuc)GlcNAc+Na]^+$ at *m/z* 534.2 detected in MS^2; and (D) MS^4 spectrum of $[GalGlcNAc+Na]^+$ at *m/z* 388.1 detected in MS^3.

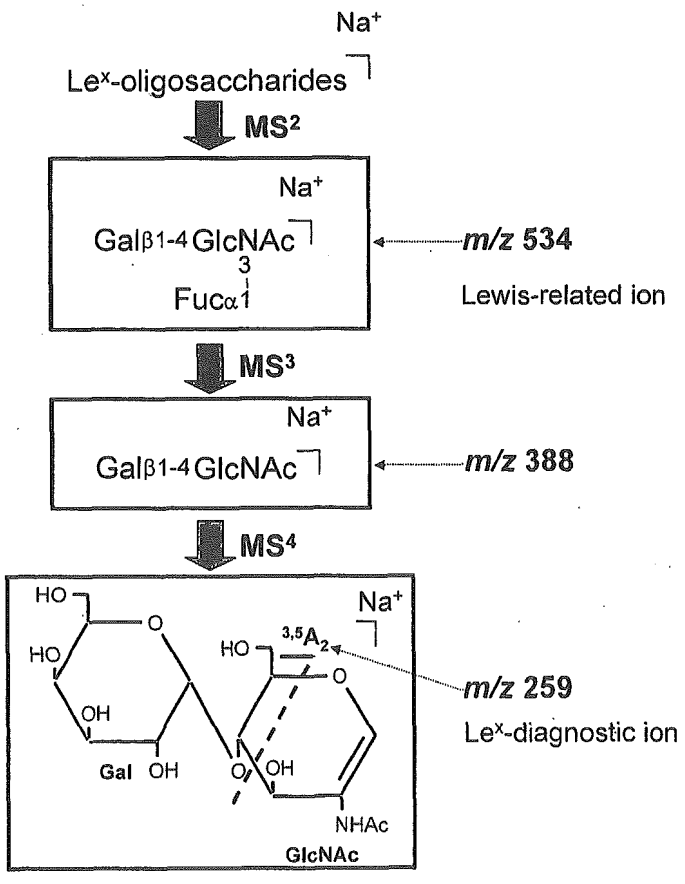

Figure 5. Proposed method for the Le^x-specific detection by ESI-MS^n.

Figure 6 shows the MS^{2-4} spectra of Le^x-asialotriantennary (oligosaccharide III). The oligosaccharide sequence can be confirmed by product ions generated by MS^2 (Fig. 6(A)). In addition to the defucosylated ion, many B- and Y-series ions, including the sodiated ion at *m/z* 534 corresponding to $[Gal(Fuc)GlcNAc+Na]^+$, were generated by MS^2. MS^3 of the sodiated $B_{2\alpha'}$ ion at *m/z* 534 yielded the sodiated $Y_{5\alpha''}$ ion at *m/z* 388 as the most intense ion (Fig. 6(B)). MS^4 of the $Y_{5\alpha''}$ ion at *m/z* 388 predictably generated the $^{3,5}A_2$ ion (*m/z* 259) (Fig. 6(C)). These results indicate that MS^3 of the sodiated ion at *m/z* 534, followed by MS^4 of the sodiated ion at *m/z* 388, can be used for the detection of the Le^x-diagnostic motif even in large and complicated *N*-linked oligosaccharides.

Specific detection and structural elucidation of *N*-linked Le^x-oligosaccharides in murine kidney by LC/ESI-MS^n

A sequential scan consisting of a full MS^1 scan, data-dependent MS^2 scan, MS^3 scan of the ion at *m/z* 534, and MS^4 scan of the ion at *m/z* 388 was applied to the specific detection and structural elucidation of Le^x-oligosaccharides in the murine kidney. In order to separate the many different oligosaccharides, including isomers, we used a LC/ITMS system equipped with a GCC. The *N*-linked oligosaccharides were released by PNGase F from the carboxymethylated proteins in the murine kidney soluble fraction. To improve the ionization efficiency and sensitivity,[25,26] the oligosaccharides were pyridylaminated, and the PA-oligosaccharides were subjected to LC/ESI-MS^n with a sequential scan. Sodiated ions were generated by a post-column reaction with 10 μM NaCl solution (2 μL/min). Oligosaccharides that yielded the

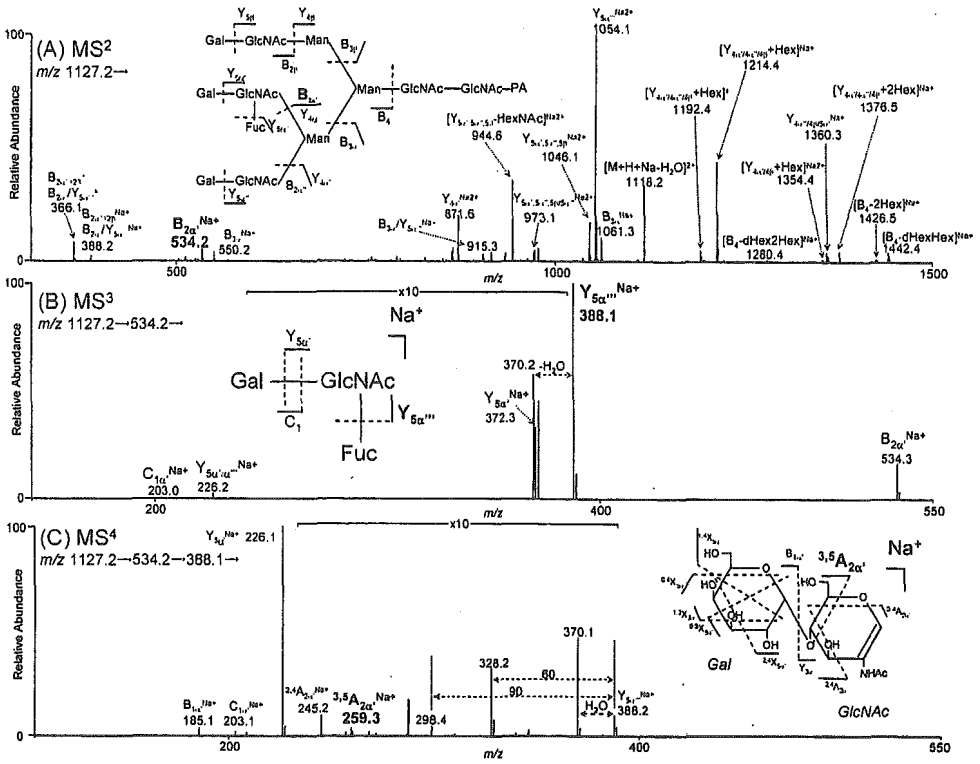

Figure 6. MS$^{2-4}$ spectra of oligosaccharide III by ESI-MS^n: (A) MS^2 spectrum of $[M+H+Na]^{2+}$ at *m/z* 1127.2; (B) MS^3 spectrum of $[Gal(Fuc)GlcNAc+Na]^+$ at *m/z* 534.2 detected in MS^2; and (C) MS^4 spectrum of $[GalGlcNAc+Na]^+$ at *m/z* 388.1 detected in MS^3.

diagnostic ions by MS$^{1-4}$ scans were presumed to be those of Le^x-oligosaccharides, and their detailed structures were elucidated by their data-dependent MS^2 spectra.

Figure 7(A) shows the total ion current (TIC) profile obtained by the full MS^1 scan of PA-labeled oligosaccharides from the murine kidney. Structures of major oligosaccharides a–i were deduced from the masses of the sodiated molecular ions measured by FTMS together with the B/Y ions generated by CID MS^2 (Table 1). Figures 7(B)–7(D) show mass chromatograms at *m/z* 534, 388 and 259, respectively, detected by MS$^{2-4}$, respectively. These chromatograms revealed that at least five kinds of oligosaccharides contain the Le^x-motif (a, b, e, f and h). Based on the masses, they were assigned to fucosylated oligosaccharides consisting of $dHex_3Hex_5HexNAc_5$ (a and f), $dHex_2Hex_5HexNAc_5$ (b), $dHexHex_4HexNAc_5$ (e), and $dHex_2Hex_4HexNAc_5$ (h) (abbreviations used here are: dHex, deoxyhexose; Hex, hexose; HexNAc, *N*-acetylhexosamine).

As an example of structural elucidation, we show the MS$^{2-4}$ spectra of oligosaccharide f in Fig. 8. In the MS^2 spectrum, we can observe the product ion $[dHex_2HexHexNAc+Na]^+$ at *m/z* 680, which can be assigned to either the Lewis b (Le^b)- or Lewis y (Le^y)-motif. As shown in Fig. 1, Le^b- and Le^y-motifs contain Le^a and Le^x as partial structures, respectively. The generation of Le^x-diagnostic ions suggests the attachment of the Le^y-motif to oligosaccharide f. Furthermore, product ions at *m/z* 1036 and 446 prove the linkage of GlcNAc at β-mannose in the trimannosyl core structure and fucosylation of the reducing terminal GlcNAc, respectively. Based on these characteristic ions, oligosaccharide f can be assigned to the bisected and fucosylated biantennary bearing the

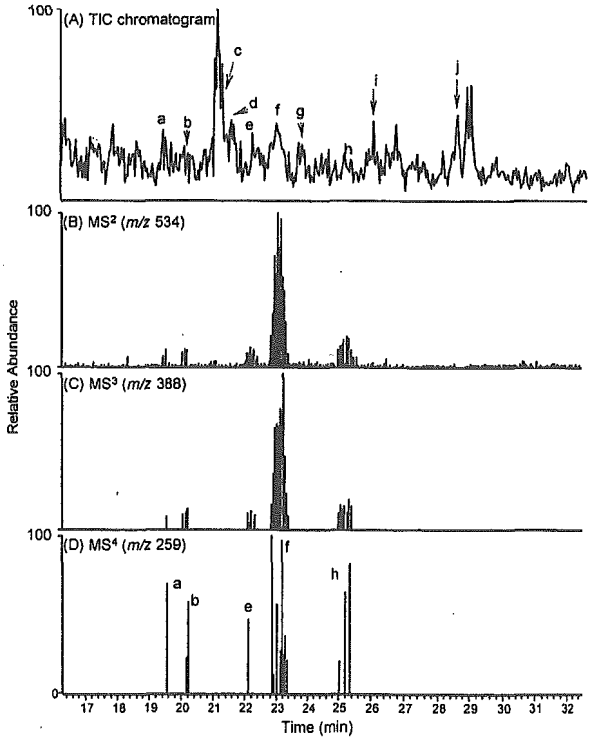

Figure 7. Specific detection of *N*-linked Le^x-oligosaccharides in murine kidney by LC/ESI-MS^n: (A) total ion chromatogram obtained by MS^1; (B) mass chromatogram of $[dHexHexNAc+Na]^+$ at *m/z* 534 detected in MS^2; (C) mass chromatogram of $[HexHexNAc+Na]^+$ at *m/z* 388 detected in MS^3; and (D) mass chromatogram of the cross-ring fragment at *m/z* 259 detected in MS^4.